Åbo Akademi University

**Shaoxia Wang**

# Surface characterization of chemically modified fiber, wood and paper

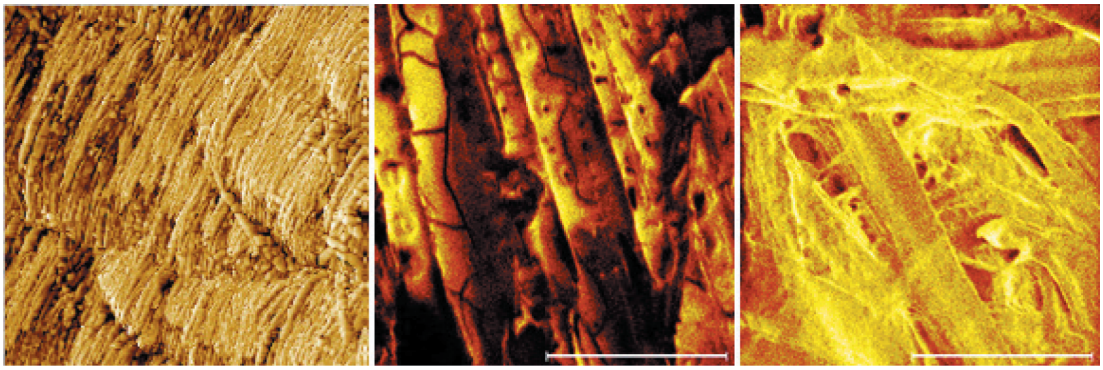

Doctoral Thesis

Laboratory of Paper Coating and Converting
Department of Chemical Engineering
Center for Functional Materials

2014

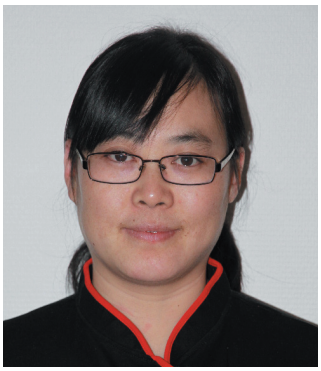

# Shaoxia Wang

Born 1978 in Shandong, China

M. Sc. in Laboratory of Physical Chemistry, Åbo Akademi, 2004.
Worked at the Laboratory of Physical Chemistry during 2004 - 2006.
Joined the Laboratory of Paper Coating and Converting in 11. 2006.

# Surface characterization of chemically modified fiber, wood and paper

Shaoxia Wang


Laboratory of Paper Coating and Converting
Center for Functional Materials
Department of Chemical Engineering
Åbo Akademi University
Åbo, Finland, 2014

## Supervised by

Professor Jouko Peltonen
Laboratory of Physical Chemistry
Åbo Akademi University, Åbo (Turku), Finland

*and*

Professor Martti Toivakka
Laboratory of Paper Coating and Converting
Åbo Akademi University, Åbo (Turku), Finland

## Reviewed by

Associated Professor Monika Österberg
Laboratory of Bioproduct Chemistry
Aalto University, Helsinki, Finland

*and*

PhD Mandla A. Tshabalala
Forest Products Laboratory, U.S. Department of Agriculture
Madison, Wisconsin, USA

## Opponent

Associated Professor Monika Österberg
Laboratory of Bioproduct Chemistry
Aalto University, Helsinki, Finland

ISBN 978-952-12-3038-7
Painosalama Oy – Turku 2014

*To Bingzhi and Yicheng*

不积跬步，无以至千里；不积小流，无以成江海。

— 《荀子·劝学》

*A journey of a thousand miles may not be achieved without accumulation of each single step, just as the enormous ocean may not be formed without gathering every brook or stream.*

— Xunzi

# PREFACE

This work was carried out within two projects: *Control of raw material and fiber properties – the key to efficient pulping* (PROPULP) during 2004-2006 at the Department of Physical Chemistry and *Nano-mediated mega value for wood and fiber-based products* (NAMEWOOD) during 2006-2008 at the Laboratory of Paper Coating and Converting at Åbo Akademi University, in collaboration with VTT technical research center of Finland. The financial supports received from the Finnish Funding Agency for Technology and Innovations (Tekes), Stora Enso Ltd, Koskisen Ltd, Millidyne Ltd, Teknos Ltd, the International Doctoral Programme in Bioproducts Technology (PaPSaT), and Magnus Ehrnrooth Foundation are gratefully acknowledged.

I would like to thank Professor Jouko Peltonen, for giving me the opportunity to work in the two projects and for his support and supervision throughout the work. I am also very grateful to Professor Martti Toivakka for his help to finalize my thesis with good comments and support. Thank you, Assistant Professor Mari Nurmi, for helping me with the thesis, especially writing the Swedish summary. Thank you also for your concerns to my personal life. I would also like to thank all my co-authors, especially, Dr. Sabine Heinemann, Adjunct professor Marjatta Kleen, PhLic. Riitta Mahlberg, PhLic. Saila Jämsä, MSc. Juha Nikkola from VTT technical research center, and Dr. Petri Ihalainen, for their contributions to the manuscripts. Technician Mr. Björn Friberg is acknowledged for checking the Swedish summary. LicFil. Jyrki Juhanoja at Top Analytica is thanked for his help with the instrumental matters and for teaching me Finnish during the internship. Our laboratory technician Pauliina Saloranta is thanked for performing the SEM measurements. Mr. Jani Kniivilä and Dr. Anders Sand are thanked for helping with all the computer problems. Thanks also to Secretary Agneta Hermansson and Christina Luojola for any official practicalities.

My great gratitude goes to Professor Qin Menghua for encouraging me to come and study in Finland. Emeritus Professor Bjarne Holmbom and Docent Anna Sundberg are highly appreciated for their assistance that made this happen.

I am also very grateful to all present and former colleagues at Physical Chemistry Department and Laboratory of Paper Coating and Converting for the pleasant work environments and the activities. Especially Helka, Joakim for being my roommates, and Dimi for interesting discussions about Finnish culture and reminding me of any holidays.

I would also like to thank all my friends both in Finland and China and elsewhere in the world for their precious friendships. Thanks to all for the supports during these years. All

the activities we had together, like traveling, cycling, barbecuing, and parties, etc, will be the great memories in my life.

Last but not least, I would like to thank my parents for their tremendous love and support in my education and life. I am also very grateful to my parents-in-law for their logistic supports while I was writing this thesis. And surely my dear husband Bingzhi Li, thank you for your love and patience during these years and for sharing my greatest moments and helping me through the difficult times. And my sweet son, Yicheng August, you are the dearest treasure to mom!

Åbo, November 2013

*Shaoxia Wang*

Shaoxia Wang

## ABSTRACT

Inorganic-organic sol-gel hybrid coatings can be used for improving and modifying properties of wood-based materials. By selecting a proper precursor, wood can be made water repellent, decay-, moisture- or UV-resistant. However, to control the barrier properties of sol-gel coatings on wood substrates against moisture uptake and weathering, an understanding of the surface morphology and chemistry of the deposited sol-gel coatings on wood substrates is needed.

Mechanical pulp is used in production of wood-containing printing papers. The physical and chemical fiber surface characteristics, as created in the chosen mechanical pulp manufacturing process, play a key role in controlling the properties of the end-use product. A detailed understanding of how process parameters influence fiber surfaces can help improving cost-effectiveness of pulp and paper production.

The current work focuses on physico-chemical characterization of modified wood-based materials with surface sensitive analytical tools. The overall objectives were, through advanced microscopy and chemical analysis techniques, (i) to collect versatile information about the surface structures of Norway spruce thermomechanical pulp fiber walls and understand how they are influenced by the selected chemical treatments, and (ii) to clarify the effect of various sol-gel coatings on surface structural and chemical properties of wood-based substrates. A special emphasis was on understanding the effect of sol-gel coatings on the water repellency of modified wood and paper surfaces.

In the first part of the work, effects of chemical treatment on micro- and nano-scale surface structure of 1$^{st}$ stage TMP latewood fibers from Norway spruce were investigated. The chemicals applied were buffered sodium oxalate and hydrochloric acid. The outer and the inner fiber wall layers of the untreated and chemically treated fibers were separately analyzed by light microscopy, atomic force microscopy and field-emission scanning electron microscopy. The selected characterization methods enabled the demonstration of the effect of different treatments on the fiber surface structure, both visually and quantitatively. The outer fiber wall areas appeared as intact bands surrounding the fiber and they were clearly rougher than areas of exposed inner fiber wall. The roughness of the outer fiber wall areas increased most in the sodium oxalate treatment. The results indicated formation of more surface pores on the exposed inner fiber wall areas than on the corresponding outer fiber wall areas as a result of the chemical treatments. The hydrochloric acid treatment seemed to increase the surface porosity of the inner wall areas.

In the second part of the work, three silane-based sol-gel hybrid coatings were selected in order to improve moisture resistance of wood and paper substrates. The coatings differed from each other in terms of having different alkyl ($CH_3$–, $CH_3$-$(CH_2)_7$–) and fluorocarbon ($CF_3$–) chains attached to the trialkoxysilane sol-gel precursor. The sol-gel coatings were deposited by a wet coating method, i.e. spraying or spreading by brush. The effect of sol-gel coatings on surface structural and chemical properties of wood-based substrates was studied by using advanced surface analyzing tools: atomic force microscopy, X-ray photoelectron spectroscopy and time-of-flight secondary ion spectroscopy. The results show that the applied sol-gel coatings, deposited as thin films or particulate coatings, have different effects on surface characteristics of wood and wood-based materials. The coating which has a long hydrocarbon chain ($CH_3$-$(CH_2)_7$–) attached to the silane backbone (octyltriethoxysilane) produced the highest hydrophobicity for wood and wood-based materials.

**Keywords**: TMP fiber, pine sapwood, heat-treated spruce, plywood, base paper, impregnated paper, surface chemistry, surface morphology, surface roughness, water repellence, water absorption, chemical treatment, sol-gel coatings, alkoxysilane, AFM, SEM, XPS, ToF-SIMS, CLSM, contact angle

## SVENSK SAMMANFATTNING

Sol-gel-beläggningar kan användas för förbättring och modifiering av egenskaperna hos vedbaserade material. Genom val av den rätta prekursorn kan veden göras vattenavstötande eller resistent mot nedbrytning, fukt eller ultraviolett strålning. Innan man kan styra barriäregenskaper som fukt- och väderbeständighet hos ett papper, krävs det dock att man förstår ytmorfologin och kemin hos sol-gel-beläggningarna.

Mekanisk massa används vid tillverkning av trähaltiga tryckpapper. Fysikaliska och kemiska fiberegenskaper som utvecklas under den valda tillverkningsprocessen, spelar en avgörande roll när det gäller slutproduktens egenskaper. En detaljerad förståelse av inverkan av processparametrarna på fiberytan kan leda till en förbättrad ekonomi hos massa- och pappersproduktionen.

Detta arbete fokuserar på fysikalisk-kemisk karaktärisering av modifierade vedbaserade material med avancerade analysmetoder. Målet var att samla mångsidig information av ytstrukturer av termomekanisk massa av nordisk gran (Norway spruce) och dess fiberväggar genom avancerade mikroskopiska och kemiska analysmetoder för att (i) förstå hur valda kemiska behandlingar påverkar sagda ytstrukturer, och att (ii) klargöra effekterna av olika sol-gel-beläggningar på strukturella och kemiska egenskaper hos vedbaserade substrat. Sol-gel-beläggningars effekter på de vattenavstötande egenskaperna hos modifierade ved- och pappersytor var av speciellt intresse.

I första delen av arbetet undersöktes effekten av kemisk behandling på strukturerna i mikro- och nanoskala hos första stegets TMP sommarvedsfibrer av nordisk gran. Kemikalier som tillsattes var buffrad natriumoxalat och saltsyra. De yttre och inre fiberväggarna hos obehandlade och kemiskt behandlade fibrer analyserades separat med hjälp av ljusmikroskopi, atomkraftsmikroskopi samt fältemissions-svepelektronmikroskopi. Resultaten visar att ytråheten hos den yttre fiberväggen ökade mest under natriumoxalatbehandlingen. Det bildades mera porer hos den exponerade inre fiberväggen än på den motsvarande yttre fiberväggen som ett resultat av kemikaliebehandlingen. Saltsyrabehandlingen verkade öka ytporositeten hos den inre fiberväggen.

I andra delen av arbetet användes tre silanbaserade, sol-gel-beläggningar för förbättring av fuktbeteende och avstötningsegenskaper hos ved- och papperssubstrat. Beläggningarna baserade sig på en silanstruktur med olika organiska kedjor. Sol-gel-beläggningarna applicerades med hjälp av spray- eller borstbestrykning. Atomkraftsmikroskopi (AFM), röntgenfotoelektronspektroskopi (XPS) och flygtidsseparerad sekundärjonmasspektrometri (ToF-SIMS) användes för analysering av

beläggningarna. Resultaten visade att sol-gel-beläggningarna har olika effekter på ytegenskaperna hos ved och vedbaserade material. Beläggningen som har en lång kolvätekedja fäst vid silanstrukturen uppvisade de mest hydrofoba egenskaperna hos ved och vedbaserade material.

## LIST OF PUBLICATIONS

I Heinemann, S., Wang, S., Peltonen, J. and Kleen, M., *Characterization of fiber wall surface structure of chemically modified TMP fibers from Norway spruce***,** Nordic Pulp and Paper Research Journal, 26 (1), 2011, 21-30.

II Wang, S., Mahlberg, R., Jämsä, S., Mannila, J., Nikkola, J., Ritschkoff, A.-C., Peltonen, J., *Surface properties and moisture behaviour of pine and heat-treated spruce modified with alkoxysilanes by sol–gel process*, Progress in Organic Coatings, 71 (3), 2011, 274-282.

III Wang, S., Malhberg, R., Mannila, J., Nikkola, J., Jämsä, S., Ritschkoff, A.-C., Peltonen, J., *Surface characteristics and wetting properties of sol-gel coated base paper*, Surface and Interface Analysis, 44 (5), 2012, 539-547.

IV Wang, S., Malhberg, R., Mannila, J., Nikkola, J., Jämsä, S., Ritschkoff, A.-C., Peltonen, J., *Surface modification and characterization of impregnated paper*, Applied Surface Science, 258 (10), 2012, 4678-4686.

V Wang, S., Jämsä, S., Mannila, J., Nikkola, J., Mannila, J., Ritschkoff, A.-C., Peltonen, J., *Treatments of paper surfaces with sol-gel coatings for laminated plywood*, Applied Surface Science, 288, 2014, 295-303.

The author has the permission to use the papers.

### Author's contribution

I The author performed the AFM measurements and analysis of the results.

II The author planned the experiments for surface analysis and performed the AFM, XPS and ToF-SIMS measurements and analysis of the results. The author wrote the manuscript and is the corresponding author.

III The author planned the experiments for surface analysis and performed the AFM, XPS and ToF-SIMS experiments and analysis of the results. The author wrote the manuscript and is the corresponding author.

IV The author planned the experiments for surface analysis and performed the AFM, XPS, ATR-FTIR and ToF-SIMS experiments and analysis of the results. The author wrote the manuscript and is the corresponding author.

V The author planned the experiments for surface analysis and performed the XPS, ToF-SIMS and AFM experiments and analysis of the results. The author wrote the manuscript and is the corresponding author.

## Supporting publications


1. Wang, S., Jämsä, S., Mannila, J., Nikkola, J., Ritschkoff, A.-C.,Peltonen, J., *Surface characteristics and water absorption of sol-gel coated impregnated paper pressed onto plywood*, Advanced Materials Research, 2011, 291-294, 159-162.

2. Wang, S., Ihalainen, P., Järnström, J. and Peltonen, J., *The effect of Base Paper and Coating Method on the Surface Roughness of Pigment Coatings*, Journal of Dispersion Science and Technology, 2009, 30, 961-968.

3. Wang, S., Mahlberg, R., Jämsä, S., Mannila, J., Nikkola, J., Peltonen, J., *Surface Characteristics of Pine and Heat-treated spruce modified with alkoxysilanes by sol-gel process*, In proceedings of 6th International Woodcoatings Congress, 2008.

4. Heinemann, S., Wang, S., Peltonen, J., Kleen, M., *Characterization of TMP fiber wall structures by microscopic techniques*, COST Action E54, Uppsala, Sweden, 2011.

5. Tshabalala, M. A., Jakes, J., VanLandingham, M. R., Wang, S., Peltonen, J. Chapter 8-Surface characterization in Rowell, Handbook of wood chemistry and wood composites, 2nd edition, CRC press, 2013.

6. Ihalainen, P., Majumdar, H., Määttänen, A., Wang, S., Österbacka, R., Peltonen, J., *Versatile characterization of thiol-functionalized printed metal electrodes on flexible substrates for cheap diagnostic applications*, Biochimica et Biophysica Acta, 2013, 1830, 4391-4397.

7. Määttänen, A., Ihalainen P., Pulkkinen, P., Wang, S., Tenhu, H., Peltonen, J., *Inkjet-printed gold electrodes on paper – characterisation and functionalisation*, ACS Applied Materials & Interfaces, 2012, 4 (2), 955-964.

8. Määttänen, A., Ihalainen P., Bollström, R., Wang, S., Toivakka, M., Peltonen, J., *Enhanced Surface Wetting of Pigment Coated Paper by UVC Irradiation*, Industrial & Engineering Chemistry Research, 2010, 49, 11351-11356.

9. Määttänen, A., Fors, D., Wang, S., Valtakari, D., Tigerstedt, M., Ihalainen, P., Peltonen, J., *Paper-based planar reaction arrays for printed diagnostics,* Sensors & Actuators: B. Chemical, 2010, 160, 1404-1412.

10. Ritschkoff, A. C., Jämsä, S., Mahlberg, R., Mannila, J., Nikkola, J., Wang, S., Peltonen, J., *Advanced wood products with nanoengineered surfaces*, In proceedings of 2010 TAPPI International Conference on Nanotechnology for the Forest Product Industry, 27-29, Sep. Espoo, Finland.

# TABLE OF CONTENTS

## LIST OF ABBREVIATIONS AND DEFINITIONS

| | |
|---|---|
| $S_1$, $S_2$, $S_3$ | Secondary wall layers |
| T | Tertiary wall |
| ML | Middle lamella |
| P | Primary wall |
| W | Warty layer |
| FE-SEM | Field Emission Scanning Electron Microscopy |
| EDS, EDX, EDXA | Energy Dispersive X-ray Spectroscopy |
| ESEM | Environmental Scanning Electron Microscopy |
| STM | Scanning Tunneling Microscope |
| AFM | Atomic Force Microscopy |
| ToF-SIMS | Time-of-Flight Secondary Ion Mass Spectrometry |
| XPS | X-ray Photoelectron Spectroscopy |
| ESCA | Electron Spectroscopy for Chemical Analysis |
| CLSM | Confocal Laser Scanning Microscopy |
| ATR-FTIR | Attenuated Total Reflectance Fourier Transform Infrared Spectroscopy |
| LM | Light Microscopy |
| TMP | Thermomechanical pulp |
| CSF | Canadian Standard Freeness |
| DDJ | Dynamic Drainage Jar |
| CWI | Cell-wall index |
| OX | Sodium oxalate buffered with oxalic acid dihydrate |
| AC | Hydrochloric acid |
| REF | Reference treatment |
| *Sq* | Root-mean-square |
| *Sdr* | Surface area ratio |
| *Ssk* | Surface skewness |
| MTEOS | Methyltriethoxysilane |
| OTEOS | Octyltriethoxysilane |
| FTEOS | Fluorocarbon-containing triethoxysilane |
| RH | Relative humidity |
| PF | Phenolic resin |
| PP | Polypropylene |

# 1. INTRODUCTION

Wood suffers from a number of disadvantages when used as a construction material. Due to its hygroscopicity, it has poor dimensional stability in changing atmospheric conditions and it is susceptible to biological attack. Potential end-uses are also restricted by changes in appearance that can appear when exposed to weathering. Therefore, wood modification is often needed to overcome these disadvantages. The aim of a modification may be to bring about improvement in decay resistance or dimensional stability, to reduce water sorption, or to improve weathering performance (Rowell 2013, Hill 2006). Modification of wood generally includes bulk (chemical, thermal and impregnation modification) and surface modification. Bulk modification can be technically problematic due to the difficulty of ensuring that the reagent is evenly distributed throughout the wood material, and that all reagent and by-products are removed at the end of the reaction. The advantage of surface modification is that it can confine the treatment reactions to the surface of the substrates, whereby the accessibility of reagent can be controlled and the modified material can subsequently be easily cleaned (Hill 2006). Surface modification of wood has been used to improve the ultraviolet stability of wood, to change the surface energy of wood (to reduce wetting, and/or improve compatibility with coatings or in wood-plastic composites), and to improve bonding between wood surfaces. Recently, it has been observed that one of the most promising methods to improve wood material properties is to surface treat wood using thin coatings with nano-hybrid materials by sol-gel technology. The mechanisms of sol-gel coatings and their applications on wood and paper substrates are described in the following sections.

Besides being a construction material, wood is also used to make pulp for paper production either in a chemical or a mechanical process. Due to high demands in the quality of mechanical printing papers, properties of mechanical pulps have become increasingly important. At the same time, the whole manufacturing process needs to be as cost-effective as possible. Therefore, process development, including improved understanding of the fiber surface characteristics, plays a key role. Both physical and chemical surface properties of pulps are very important since they influence fiber charge, fiber bonding, wettability, adsorption, adhesion and consumption of papermaking chemicals. In mechanical pulping, it has been found that morphologically different fibers react in different ways to refining and defibration conditions (Pöhler 2003, Heikkurinen 1999). Not only the fiber dimensions, wood density and dry solids content influence the wood behavior in mechanical processing, but also the fiber structure will contribute to the defibration result. On the other hand, the fiber surfaces can be influenced by the refining process, e.g. the refining energy input, refining intensity, and a possible pretreatment of the wood chips with steam or chemicals prior to refining. In this thesis, the chemicals selected for treatment of thermomechanical pulp (TMP) fibers were buffered sodium

oxalate and hydrochloric acid. The buffered sodium oxalate was used for targeting more energy-efficient TMP-production. About 25% reduction in the specific energy demand in refining was obtained by the oxalate treatment of chips prior to refining. The effect of sodium oxalate on the refining response of fibers and fiber chemistry has been reported in the literature, but the morphological changes of the fiber surfaces induced by a chemical pretreatment prior to refining have not previously been investigated.

The overall aims of this work were, through advanced microscopy and chemical analysis techniques, (i) to collect versatile information about the surface structures (inner ($S_2$) and outer (ML/P) walls) of Norway spruce TMP fiber walls and understand how they are influenced by the selected chemical treatments, and (ii) to clarify the effect of sol-gel coatings on surface structural and chemical properties of wood-based substrates. A special focus was on understanding the effect of sol-gel coatings on the water repellency of modified wood and paper substrates.

# 2. BACKGROUND

Wood can be botanically categorized into softwoods and hardwoods. Softwoods are those woods from gymnosperms, which generally have needle-like leaves such as pine (*Pinus*) and spruce (*Picea*). Hardwoods are those woods from angiosperms such as maple (*Acer*), birch (*Betula*), and oak (*Quercus*). Both softwoods and hardwoods contain two distinct zones, sapwood and heartwood. Sapwood gives structural support to the living tree and is located adjacent to the bark and functions as the conduction of sap and storage and synthesis of biochemicals. The primary photosynthates in sapwood are starch and lipids. Heartwood is found to the interior of the sapwood with a darker color. Heartwood functions as a long-term storage of biochemicals, which are known collectively as extractives. The extractives in heartwood protect the tree against biological attack, lower the water content and act as fungicides (Wise 1952). In general, wood is heterogeneous material with respect to its anatomical, physical, and chemical properties.

In this work, the wood samples are Norway spruce (*Picea abies*) and Scots pine (*Pinus sylvestris*). They both are softwood species which mainly consists of tracheids, parenchyma and epithelial cells. The moisture content and permeability of sapwood is generally higher than that of heartwood. The difference between the permeability of heartwood and sapwood has been reported to be greater in pine than spruce (Elowson 2003).

## 2.1 Wood cell wall structure and chemistry

It is known that the cell walls in wood are of key importance for the performance of wood-based products. The cell wall of wood consists of a number of different layers shown in Figure 1: the middle lamella (ML), the primary wall (P), and the secondary wall. The ML is located between the P walls of adjacent cells and binds the cells together. This layer is the outermost layer of the cell wall and lignified. The P wall is a thin and elastic layer composed of randomly orientated (microfibril angle from 0º to 90º relative to the long axis of the cell) cellulose microfibrils. The secondary layer can be divided into three sub-layers: the outer layer of the secondary wall ($S_1$), the middle layer of the secondary wall ($S_2$), and the inner layer of the secondary ($S_3$). The $S_3$ layer is sometimes also referred to as the tertiary wall (T). These cell layers differ from one another with respect to their structure as well as their chemical composition. The outer layer, $S_1$, is a thin layer (consists of 3–4 lamellae) and is characterized by a large microfibril angle (50º–70º). The $S_2$ layer is the thickest secondary cell wall layer (30–150 lamellae) and has the greatest influence on many properties of the cell wall and the macroscopic properties of the wood (Panshin 1980, Rowell 2013). It has a lower lignin percentage and a low microfibril angle (5º–30º). The $S_3$ layer is a relatively thin layer with several lamellae of microfibrils.

The microfibril angle of this layer is >70º. It has the lowest percentage of lignin among the secondary layers. In certain cases, for example, conifer tracheids and some hardwood cells, the inside of the $S_3$ layer is covered with a thin membrane called the warty layer (W).

The wood cell wall mainly consists of cellulose, hemicellulose, lignin and extractives. There are many excellent descriptions about the structure and function of these components. Only a brief introduction will be given here.

Cellulose is homopolysaccharide composed of glucose chains. The average degree of polymerization for wood cellulose is 9000–15,000. It constitutes approximately 40%–45% of both softwoods and hardwoods. A number of cellulose chains are closely associated through extensive hydrogen bonding networks to form the microfibrils. Due to the high crystalline nature of the microfibrils, the cellulose component is relatively unreactive and thermally stable.

Hemicelluloses are polysaccharides composed of a number of different sugar units, mainly of glucose, xylose, galactose, mannose and arabinose (Fengel 1989). The typical content of hemicelluloses in softwoods and hardwoods is 25%–30% and 30%–35% of the wood dry solids, respectively. The structures of the different types of hemicelluloses vary with the plant species. The chemical and thermal stability of hemicelluloses is generally lower than that of cellulose, presumably due to their amorphous nature and lower degree of polymerization (100–200). Hemicellulose contains the highest proportion of the accessible OH groups in the cell wall.

Lignin is an amorphous phenolic polymer with an irregular complex chemical structure. The structural building blocks of lignin are joined together by C–O–C and C–C linkages. The lignin content of softwoods and hardwoods is typically in the range of 25%–30%, 20%–25%, respectively. Compared to cellulose and hemicellulose, lignin has a lower concentration of OH groups.

Extractives are extractable chemicals in the wood mainly consisting of fats, fatty alcohols, terpenes, fatty acids, phenols, steroids, resin acids, rosin and waxes. The contents of extractives in the wood vary from 0.5% to 20% depending on the species. In wood chemical modification processes, extractives can be problematic due to their leachability to the medium. Also, migration of extractives can occur during the heat treatment of wood.

The three main structural wood constituents, cellulose, hemicellulose, and lignin, are not uniformly distributed in wood cells, and their relative mass proportions can vary widely

depending on the morphological region and age of the wood. The different wood cell wall layers can be identified for instance with light microscopy, atomic force microscopy, scanning electron microscopy, and transmission electron microscopy (Molin 2004, Fromm 2003, Duchesne 1999, Bardage 2004).

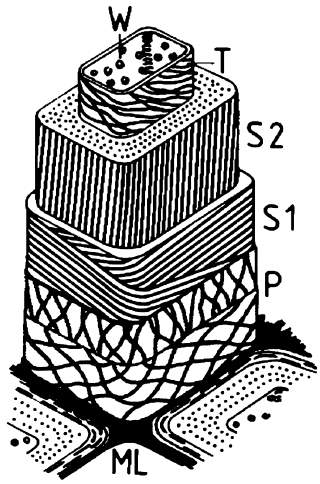


**Figure 1.** Model of the cell wall structure of softwood tracheids and hardwood libriform cells. ML: middle lamella (0.1–1 µm), P: primary wall (0.1–0.3 µm), $S_1$: outer secondary wall (0.1–0.2 µm), $S_2$: secondary wall (1–5 µm), T: tertiary wall or inner secondary wall ($S_3$) (0.1 µm), W: warty layer (Fengel 1989).

In terms of wood modification, in wood cell wall the main sites of reaction are hydroxyl groups of the cell wall polymers (cellulose, hemicellulose and lignin). For successful modification, deposition of the modifying agent in the cell wall is crucial.

### 2.2 Thermomechanical pulping

The mechanical pulping was developed in Germany by F.G. Keller in the 1840s (Sjöström 1993). Today, the thermomechanical pulping (TMP) process is the dominating refiner-based mechanical pulping process. In the TMP process, pulp is made by heating the chips with steam and mechanically separating the fibers in a pressurized refiner. The refining process generally includes two stages: fiber separation and fiber development which can occur simultaneously (Karnis 1994). In the fiber separation stage, wood chips are broken down to smaller particles, whereas fiber development proceeds via delamination and peeling of the fiber surface. Basically, the outer fiber wall layers, i.e. middle lamella, primary wall and outer secondary wall, are peeled off leaving the inner secondary wall exposed.

Mechanical pulp fibers have very heterogeneous structure and their composition depends on both the wood species and the processing method. The quality of mechanical pulp is determined by the inherent properties of the pulp fibers, such as the surface ultrastructure and chemical composition, and their physical properties.

### 2.3 Paper

Paper is a versatile material made from various fibers which are typically derived from wood, rags or grasses. Paper is used principally for printing, writing and many other applications. Based on the classification used by the European forest industry companies, paper can be mainly divided into: printing and writing papers, paperboards, tissue and specialty papers. Printing and writing papers are those papers used for newspapers, magazines, catalogs, books, copying, and printing. Paperboards are usually used for packaging. Tissues are mainly used for hygiene purposes. Specialty papers typically have specific characteristics such as strength, thickness, porosity, absorptivity, which target particular end-use applications (Paulapuro 2000). In the current study, base paper and impregnated paper are used as laminates for plywood and can be considered to be specialty papers.

### 2.4 Plywood

Plywood is one of the most widely used wood composites. It is made by gluing thin wood veneers together. Plywood is in many cases used instead of plain wood because of its high strength and its resistance to cracking and shrinkage. Hardwood plywood is primarily used for decorative purposes while softwood plywood is usually applied in the building industry. The modification of plywood has been done with an overlayed resin impregnated paper on top of it (Fahey 1971). It has also been reported that the wear and climatic resistance for plywood can be achieved by thermosetting resin coating (e.g. phenol-formaldehyde). The thermosetting resins are applied on to the plywood by pressing under high temperature and pressure (Kuusipalo 2001). The coated plywood is primarily used in concrete cast moulds, horse boxes, flooring of vehicles and claddings. However, the disadvantages of coated thermosetting resins are their limited wear resistance, brown color, limited coloring possibilities, and limited water resistance. A better water and wear resistance and appearance were found by Tervala et al. by using an alternative thermoplastic coating (e.g. polyethylene and polypropylene) (Tervala 1999).

### 2.5 Thermal modification of wood

The thermal modification, usually performed between 180°C and 260°C, has been used to improve the dimensional stability and decay resistance of wood. The first scientific study of heat treated wood was carried out by Stamm and Hansen in the 1930s in

Germany by heating the black gum at 205°C to reduce its hygroscopicity (Stamm 1937). The most recent commercialized thermal treatment processes in Europe are the ThermoWood process in Finland, the Perdure and Retification processes in France, and the Plato process in the Netherlands. The thermal treatment generally changes the chemical, physical and biological properties of wood depending on the process variables: time and temperature of treatment, wood species, sample dimensions, catalysts used and system closure.

The physical changes include changes in color, dimensions, crystallinity and mechanical properties as well as a mass loss (Hill 2006). Usually, a darkening of the wood occurs and wood becomes more stable than untreated wood after a treatment. Ayadi et al. reported that the color stability of thermally modified wood is better than for control samples in accelerated weathering tests (Ayadi 2003). However, Syrjänen et al. found that the color of heat-treated samples will nonetheless fade if they are exposed to exterior conditions (Syrjänen 2000). Hietala et al. reported an increase in the microporosity of the cell wall (the average pore size was of the order of tens of nanometers) resulting from the steam heating at temperatures in excess of 180°C due to component removal (Hietala 2002). The benefits of heat treatment lie in the increased dimensional stability, reduced hygroscopicity and improved decay resistance. However, the heat treatment at high temperatures may cause reduction in strength, toughness and abrasion resistance (Chang 1978). The chemical changes in wood due to thermal modification are complex and dependent on the treatment conditions. The main components of wood degrade in different ways under heat. It is generally believed that cellulose and lignin degrade more slowly and at higher temperatures than the hemicelluloses. The extractives degrade more easily and evaporate from the wood during the heat treatment (Nuopponen 2003).

In this work, the heat-treated spruce (Thermo-S®, S is stability) for sol-gel coatings was manufactured by the ThermoWood process developed by VTT technical research center of Finland (ThermoWood® handbook 2003). The ThermoWood process can be briefly divided into three main phases as shown in Figure 2. Phase 1 is the temperature increase and kiln drying by using heat and steam in air. Steam is used as vapor membrane to prevent cracking of the wood and to facilitate chemical changes taking place. The wood moisture content is reduced to nearly zero at the end of this stage. Phase 2 is intensive heat treatment at a temperature of 185-225°C (the peak temperature is dependent on the desired end use of the material) for 2-3 hours. Phase 3 is cooling and moisture conditioning. The temperature is reduced to 80–90°C by water spray systems. The wood material is therefore re-moistured to a workable moisture content level of over 4%. A detailed description of the industrial-scale heat-treatment process for wood can be found in the ThermoWood® handbook.

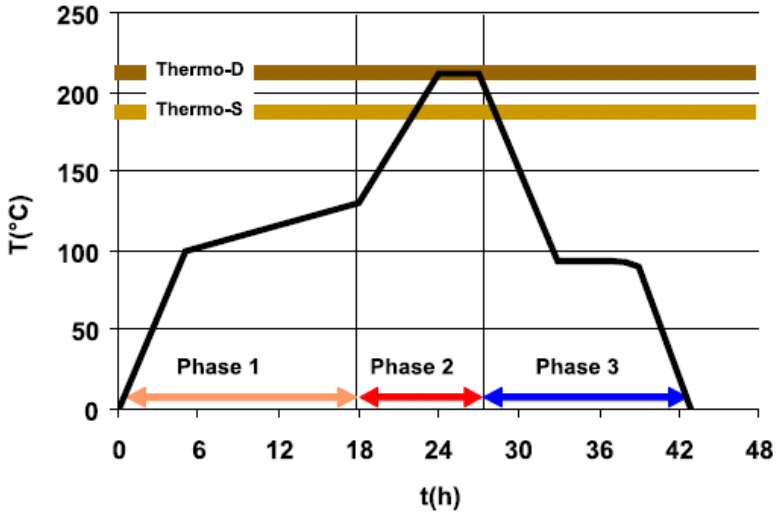


**Figure 2.** Temperature-time diagram of a wood heat-treatment process (ThermoWood® handbook 2003).

The main chemical changes occurring in the ThermoWood heating process are thermal degradation of hemicelluloses. As a result of the heat treatment, the biological durability, dimensional stability, thermal insulation properties and decay resistance of wood are improved. In addition, the equilibrium moisture content and water uptake of wood is reduced. However, the bending and splitting strength of wood can slightly decrease by the high treatment temperature. ThermoWood-treated wood is usually unable to resist weathering effects; therefore, the surface needs to be protected by a surface coating to prevent color changes and other effects from weather exposure.

### 2.6 Modification of wood and paper substrates by sol-gel technology

Modification of wood has been done chemically, thermally and through other processes. An excellent elucidation about wood modification is in a book by Hill (Hill 2006). Various types of chemical compounds and treatments have been used in the modification of wood properties including anhydrides, acid chlorides, carboxylic acids, alkyl chlorides, isocyanates, aldehydes, nitriles, lactones, epoxides, elevated heat and plasma treatment (Rowell 1981, Rowell 1985, Militz 1997, Mahlberg 1998, Ritschkoff 2003, Jämsä 2001).

Over the last years, a wide variety of inorganic and organic silicon compounds have been used for wood modification with attempts to improve its fire resistance, water repellence, fungal decay resistance, durability and to reduce the fungal disfigurement (Saka 1992, Saka 1997, Saka 2001, De Vetter 2009a, b, Tshabalala 2003a). The wood modification with the inorganic and organic silicon compounds is well reviewed by Mai and Militz

(Mai 2004a, b). In this chapter, the wood and paper modification with alkoxysilanes is briefly reviewed.

Treatment of wood with alkoxysilanes has been found promising to improve wood material properties as well as to provide new properties into wood-based substrates. The effect of alkoxysilanes on wood moisture behavior and dimensional stability, anti-mold, anti-fungal and weathering properties has been reported in literature (Saka 2001, Tshabalala 2003a, b, Tshabalala 2007, Tshabalala 2009, Donath 2006, Donath 2007).

The alkoxysilanes can be applied to wood by different approaches. In one approach, the hydrolysis of the alkoxysilane is initiated by the bound water and free water in the wood (Saka 1992, Ogiso 1993). In another approach, silanes are first hydrolysed in a batch reactor before treatment of wood (Mai 2004a). The main sites of reaction for wood and paper substrates are the hydroxyl groups. In general, the reactions of the alkoxysilane with the substrates by a sol-gel process involve four steps as shown in equations 1-3, which begin with hydrolysis of the three alkoxyl groups, followed by condensation to oligomers. The oligomers form hydrogen bonds with hydroxyl groups of the substrate. Finally, during drying or curing, a covalent bond is formed with the substrate.

$$R'Si(OR)_3+H_2O\rightleftarrows(OR)_2R'Si(OH)+ROH \quad (1)$$

$$R'Si(OH)(OR)_2+R'Si(OR)_3\rightleftarrows(OR)_2R'SiOSiR'(OR)_2+ROH \quad (2)$$

$$R'Si(OH)(OR)_2+R'SiOH(OR)_2\rightleftarrows(OR)_2R'SiOSiR'(OR)_2+H_2O \quad (3)$$

In above, R refers to a methyl or an ethyl group and R' refers to e.g. an alkyl or a fluoroalkyl chain, or an amino or epoxy group. The alkoxysilanes can be applied to wood or paper by impregnation or by surface treatment with dip, spill or spin coating, spraying, brushing or roll coating. The surface treatment is usually carried out with a silane water-alcohol solution in a concentration range of 0.5–2% by weight (Brochier Salon 2005). Typically, thickness of these sol-gel coatings ranges from 0.1 to 10 µm depending on the coating chemistry and the coating technique used. Because of the very thin coatings, the surface properties can be modified without changing the bulk substrate properties or appearance. In addition to the sol-gel deposition methods, surface modification of wood can be also accomplished by plasma-enhanced chemical vapor deposition methods (Denes 1999, Podgorski 2001, Bente 2004).

A hydrophobic surface can be obtained by employing organically modified alkoxysilanes (organosilane) with long-chained aliphatic or highly fluorinated hydrocarbon substituents by a sol-gel route (Mahltig 2005, Textor 2010, Wang 2011). Factors which contribute to the ability of an organosilane to generate a hydrophobic surface are its organic

substitution, the extent of surface coverage, residual unreacted groups (both from the silane and the surface) and the distribution of the silane on the surface. The advantage of silanes over other water repellents, such as oils or waxes, is that the sorption behavior of wood is only marginally influenced.

Silane based sol-gel materials have also been applied onto paper substrates, for example, to enhance the resistance of paper against environmental effects caused by water or heat (Yoldas 1998, Iwamiya 2000, Kiuberis 2003, Yagi 2005). A recent study by Yagi et al. showed that tensile strength and water repellency of paper was improved after treatment with a methyltrimethoxysilane oligomer (Yagi 2005). Another study showed that coating of paper with sol-gel silica layers containing bound dyes improved the leaching stability (Trepte 2000). Ly et al. reported that by grafting of cellulose with fluorine-bearing silane coupling agents, it is possible to achieve a highly hydrophobic non-penetrating surface (Ly 2010).

# 3. SURFACE CHARACTERIZATION

## 3.1 Surface energy and wetting of a rough surface

***Surface energy***

Surface energy or surface free energy is conventionally defined as the work required to build a unit of area of a given surface (Oura 2001). Contact angle measurements can be used to determine the surface energy of a material. The term surface energy or surface free energy is occasionally preferred for solid surfaces, while the term surface tension is usually used for liquids and vapors. The surface energy of a solid can be determined by, e.g., Zisman's plot, Girifalco-Good, Fowkes, Owen-Wendt, Wu, and Van Oss-Chaudhury-Good methods. These methods have been reviewed in literature (Adamson 1967, Zenkiewic 2007, Girifalco 1957, Good 1960, Fowkes 1964, Owens 1969, Wu 1971, Vanoss 1988, Correia 1997). In this thesis, Fowkes's equation was used for calculation of surface energy of sol-gel coated impregnated paper (paper IV). The total surface energy and surface dispersive and polar components are calculated using the geometric mean method. The geometric mean method (also known as the Fowkes, extended Fowkes, Owens and Wendt method) is suitable for characterization of non-polar and moderately polar substrates such as plastics, rubber, polymer films and paper.

***Wetting of a heterogeneous surface***

Wetting refers to the study of how a liquid deposited on a solid (or liquid) substrate spreads out. It is known that the wettability of a solid surface by a liquid droplet is strongly affected by both intrinsic chemical properties and surface roughness of the solid surface. The wettability of a rough solid surface is frequently represented by an apparent contact angle of a liquid droplet on the surface. The relationship between the apparent and the intrinsic contact angle can be described by the following two models. The Wenzel model (Wenzel 1949) is applied to a rough surface which is fully wetted by a liquid droplet:

$$\cos\theta^m = r\cos\theta ,$$

where $\theta$, $r$, and $\theta^m$ are the intrinsic contact angle on the solid surface, the ratio of the actual area of the rough surface to the projected area, and the apparent contact angle on the wetted surface, respectively. The Wenzel equation states that a rough hydrophilic surface should appear more hydrophilic and a rough hydrophobic surface more hydrophobic than a smooth surface with the same chemical composition. Cassie-Baxter model (Cassie 1944) is introduced when a liquid droplet is placed only on top of the rough features of the surface (composite surface):

$$\cos\theta^m = -1 + \phi_s(1+\cos\theta),$$

where $\phi_s$ and $\theta^m$ are the solid area fraction of the solid surface (solid fraction) and the apparent contact angle on the composite surface, respectively. In this model, air is entrapped below the liquid droplet. The influence of the surface geometry on the entrapment of air was demonstrated by Wapner et al. (Wapner 2002). Bico et al. observed air entrapment when surface roughness was of the order of 30 μm (Bico 2002).

For a chemically heterogeneous surface, the Cassie model is typically used to describe the wetting (Cassie 1948):

$$\cos\theta^m = f_1\cos\theta_1 + f_2\cos\theta_2,$$

where $\theta^m$ is the apparent contact angle on the ideally flat two-component surface, $f_1$ and $f_2$ are the area fractions of material 1 and 2, $\theta_1$ and $\theta_2$ are the Young contact angles on pure materials 1 and 2. According to both Wenzel and Cassie models, surface roughness enhances the effects of hydrophobic or hydrophilic behavior (Hay 2008, Kim 2009, Spori 2008). However, both the Wenzel and the Cassie equations are approximations, and they are valid only when the scale of the roughness/heterogeneity is small compared to the length of the three phase contact line (Nosonovsky 2007, Brandon 2003, Iliev 2003).

### 3.2 Microscopic methods

A variety of microscopic and spectroscopic methods have been used for characterization of wood, paper and fibrous surface ultrastructure and chemical composition. Characterization of surface properties of pulp, paper and wood is very complex. Usually, several techniques are combined in order to obtain adequate information about the surface. This and the following chapters describe the main surface analysis techniques used in this thesis.

***Light Microscopy***

Light microscopy (LM) involves passing visible light transmitted through or reflected from the sample through a single or multiple lenses to allow a magnified view of the sample (Abramowitz 2007). Different techniques, such as bright field, oblique illumination, dark field, dispersion staining and phase contrast, can be used to improve the specimen contrast or to highlight certain structures. The light microscopy has in the past played a very important role in the study of wood anatomy and in investigations of the structure of fibers and paper. Light microscopy provides low magnification (8–1000X) of fibers and textiles that can be used to examine fiber surface characteristics and

measure their shape and dimensions. In addition, it is useful for the determination of the construction and function of fibrous assemblies; diagnosis of chemical and microbial damage, and evaluation of processing defects and mechanical degradation. The morphology of mechanical pulp fiber surfaces has been studied by light microscopy using staining and polarization (Jayme 1970a, b; Werthmann 1993a, b). The disadvantages of light microscope include low magnification (1000-2000X) and resolution (200 nm) when analyzing sub-micron size features.

***Confocal Laser Scanning Microscopy***

The confocal laser scanning microscopy (CLSM) was first invented by Minsky in 1950s and became commercially available 1987 (Minsky 1988). In this thesis work, a Leica CLSM was used for capturing 3D topographical images of wood and paper samples. The system consists of a conventional Leitz Diaplan light microscope to which an argon-ion laser unit (operating at wavelengths of 488 nm & 514 nm) is coupled, comprising beam generation and photodetector units, a scanning system, control panel and monitors. All functions are controlled by a fast central processing unit (Moss 1993). The CLSM differs from the conventional light microscope in that the optical system of the CLSM contains two pinholes whereas in the conventional LM the whole field of view is illuminated and simultaneously imaged directly to the eye or to a monitor. In CLSM only the focal plane is scanned point-by-point in raster fashion. The advantage of CLSM over the other types of optical microscopes is that it allows 3-D imaging of thick and opaque specimens, such as wood surfaces (Rowell 2013). The CLSM also provides a measurement of surface roughness at large scale in comparison with AFM. Nevertheless, the CLSM has a limit in a detailed examination of fine structures such as fibrillar material.

The CLSM has been widely used in the studies of fiber morphology, drying process of wet webs, external fibrillation in different fibers, and fibril orientation in the $S_2$ layer of wood fibers, wet fiber flexibility, paper cross-section analysis, chemical distribution across the fiber wall (Nanko 1989, Ylikoski 1992, Jang 1998, Yan 2008, Ozaki 2005, Li 2005). The CLSM has also been found to be useful in study of the surface roughness of coated wood and paper (Tshabalala 2007, Enomae 2006) and in examining wood-coating interface and macro-fracture in wood (Singh 2004, Dill-Langer 2004).

***Scanning Electron Microscopy***

Scanning Electron Microscopy (SEM) was first developed in the 1930s and commercialized in 1960s. Compared to light microscopy, SEM has much higher magnification, up to 100,1000X. The sample surface is imaged by scanning it with a focused beam of high-energy electrons in a raster scan pattern. When the electron strikes the specimen, secondary electrons, backscattered electrons, diffracted backscattered electrons, photons, visible light, and heat, is generated through electron-sample

interactions and collected in detectors which convert them to a signal that is processed into an image. These signals include secondary and backscattered electrons, which are commonly used for imaging samples. Secondary electrons are most valuable for investigating the external morphology and topography of a sample. The contrast in the image is determined by the surface morphology. In general, a larger number of secondary electrons are displayed as bright spots in the images. Small projections on the sample surface appear brighter than flat areas. Backscattered electrons are most valuable for illustrating contrast in composition in multiphase samples, i.e. the image shows the distribution of different chemical phases in the specimen surface. With a field emission electron emitter (FE), it is possible to obtain images with high magnification. FE-SEM has a depth resolution of 1–5 μm and lateral resolution of 5 nm. In addition to imaging, elemental analysis can be performed by detection and measurement of X-rays, which is commonly referred to as Energy Dispersive X-ray Spectroscopy (EDS, EDX or EDXA). EDS can provide quantitative analysis of elemental composition with a sampling depth of 1–2 microns. The detection limit is 0.1–0.5 wt%. The samples for SEM images need to be conductive in order to prevent charging artifacts and consequent loss of image quality. Therefore, most electrically insulating samples are coated with a thin layer of conducting materials, commonly carbon, gold, or some other metal or alloy. The recent development in SEM is environmental scanning electron microscopy (ESEM), which allows the introduction of a gaseous environment in the specimen chamber and no pre-coating of the insulating samples is required.

One of the first fields in which the scanning electron microscope was consistently applied in research was in wood and paper technology, and results have been described in a number of publications. The surface structural properties of TMP fibers and fines observed by SEM have been reported by Lidbrandt 1980, Johnsen 1995, Braaten 1997, Reme 1998, Kangas 2004, Fernando 2008, Fernando 2011, Daniel 2009. Buchanan and Washburn described the use of SEM for the examination of the surface and tensile fractures of chemical fiber handsheets (Buchanan 1962). Forgacs and Atack used scanning electron microscopy to observe the distribution of chemical wood pulp and groundwood through the thickness of newsprint (Forgacs 1961). Adusumalli and Raghavan et al. have studied the deformation of single fiber in transverse direction by using in situ SEM micro-indentation (Adusumalli 2010). Fromm and Rockel et al. reported a technique based on the mercurization of lignin and the subsequent visualization of mercury by FE-SEM combined with a back-scattered electron detector. Fromm found that the lignin distribution across the different layers of the wood cell wall could be visualized by SEM (Fromm 2003). Peng et al. have utilized SEM together with AFM and XPS to study the surface characteristics of cellulose fibers after laccase and alkali treatments (Peng 2010). SEM-EDX was used to detect the silicon distribution in the wood cells by measuring cross-sections of wood (Tingaut 2006, Donath 2004, Donath

2006). SEM micrographs of sol-gel coatings on cellulose fiber and wood have also been reported (Tomšič 2008, Tshabalala 2003a, b, Tshabalala 2007).

***Atomic Force Microscopy***

The atomic force microscopy (AFM) was first developed by Binning et al. in 1986 to overcome a basic drawback with Scanning Tunneling Microscope (STM) which can only image conducting or semiconducting surfaces (Binning 1986). Different from optical and electron microscopes which use light or electrons, in AFM, a probe consisting of a sharp tip located near the end of a cantilever is raster scanned across the surface of a specimen using piezoelectric scanners. The cantilever is typically Si or $Si_3N_4$ with a tip radius from a few to tens of nm. AFM measures the attractive or repulsive forces between the tip and the sample. As the raster-scan drags the tip over the sample, the vertical deflection of the cantilever is detected and monitored with a laser beam and a photodiode detector (Meyer 1990). Three modes of operation; contact mode, non-contact mode, and intermittent contact or tapping mode can be used to produce a topographic image of a surface. A detailed description of AFM and its basic modes was elaborated in the book by Greg Haugstad (Haugstad 2012).

The AFM measurements in this thesis were performed in tapping mode. In tapping mode, in addition to topographical images, the phase images were also captured by measuring the phase-shift caused by the changes in the phase angle of the cantilever probe interacting with the sample. The phase imaging is useful to investigate surface fine features which are obscured by rough topography, and to detect material properties, such as stiffness, adhesion, elasticity, and chemical composition.

A set of roughness parameters has been developed for versatile characterization of surface properties in three dimensions. The parameters are defined by the ISO 25178 standard, which is the first international standard taking into account the specification and measurement of 3D surface texture (ISO 25178). In this thesis, the following roughness parameters are used: Root-Mean-Square (RMS) roughness ($S_q$), Skewness ($S_{sk}$), and Kurtosis ($S_{ku}$). The RMS parameter is the most widely used amplitude roughness parameter, and it expresses the standard deviation of height. The surface skewness describes the asymmetry of the height distribution within the sampling area. A skewness value equal to 0 represents a Gaussian-like surface. A negative value refers to a surface-porous sample, i.e. the valleys dominate over the peak regimes, whereas, a positive value indicates a non-porous surface, i.e. the local maxima dominate over the valleys. The surface kurtosis describes the peakedness of the surface topography. A Gaussian value for this parameter is 3.0, smaller values indicate broader height distribution and vice versa for values larger than 3.0.

Measured surface roughness is scale dependent, which means that for an accurate analysis both the amplitude and lateral spacing of surface heights should be considered when determining the surface roughness. Detailed description of a method for surface roughness analysis of pigment coatings at different length scales was elaborated by Järnstöm (Järnström 2010).

An advantage of AFM over SEM is that it does not require any special treatments to the samples and it has a much higher resolution. AFM has been widely used in material science to obtain high-resolution 3D images of a surface at different scales: from atomic (1 Å) to micrometer scale with a lateral resolution of ~1 nm and the depth/vertical resolution of ~0.1 nm. AFM imaging has been successfully applied to pulp, paper and wood materials, e.g. for the surface morphological studies of mechanical pulps, revealing different fiber wall layers and components(Kangas 2004, Kleen 2003, , Hanley 1994; Börås 1999; Koljonen 2003, Österberg 2006; Snell 2001; Kangas 2004; Gustafsson 2004; Stenius 2008; Li 2010). The AFM has also been used to study sol-gel films/coatings and the phase separation of organic-inorganic nanocomposite hybrid coatings (Tshabalala 2003a, Amerio 2005).

### 3.3 Spectroscopic methods

***Attenuated Total Reflectance Fourier Transform Infrared Spectroscopy***

Attenuated total reflectance Fourier transform infrared spectroscopy (ATR-FTIR) was first introduced in the 1960s. Infrared spectroscopy provides information about molecular vibration, and permits the identification of functional groups. ATR is a sampling technique used in conjunction with infrared spectroscopy where a beam of infrared light is passed through the ATR crystal in a way that it reflects at least once off the internal surface in contact with sample. This reflection forms the evanescent wave which extends into the sample. The penetration depth of the infrared beam into the sample is between 0.5 and 2 micrometers. Therefore, this technique is not as surface sensitive as XPS and ToF-SIMS. A detailed description of the fundamentals and applications of ATR-FTIR can be found elsewhere (Stuart 2004). ATR-FTIR has been used to characterize the chemical structure of alkoxysilane modified wood (Tingaut 2006, Tshabalala 2003a).

***X-ray Photoelectron Spectroscopy***

X-ray photoelectron spectrometers became commercially available in 1969 and were first used to study polymers. X-ray photoelectron spectroscopy (XPS), also known as electron spectroscopy for chemical analysis (ESCA), is a highly surface sensitive technique for analyzing the chemical composition of the outermost layer of a sample with a surface analysis depth of 5–10 nm and a lateral resolution of 10 μm. In XPS, the sample is irradiated with x-rays usually generated by either Mg Kα (1253.7 eV) or Al Kα (1486.6

eV) excitation sources under ultra-high vacuum conditions. The photons interact with atoms in the surface region, resulting in emission of photoelectrons whose energies are characteristic of the elements present on the surface. This technique provides a total elemental analysis, which can be used to identify the elements qualitatively and quantitatively, with the exception of hydrogen and helium. XPS can also provide chemical bonding formation of a solid surface (Sain 2000).

XPS has been used in the study of wood surfaces coated with multifunctional alkoxysilanes by sol-gel deposition. A covalent bond was observed between extracted wood and alkoxysilanes by XPS C1s high resolution spectra (Tshabalala 2003a, b, Tshabalala 2007). XPS has also been used to study the elemental and chemical composition of pulp fibers (Koljonen 2003, Koljonen 2004, Gustafsson 2004, Börås 1999, Mustaranta 2000, Mosbye 2003, Kangas 2007). By XPS, the coverage of lignin and extractives on the mechanical pulp surface was estimated by detection of oxygen and carbon before and after extraction of the sample with a solvent, such as acetone or dichloromethane.

***Time-of-Flight Secondary Ion Mass Spectrometry***

Time-of-flight secondary ion mass spectrometry (ToF-SIMS) uses a pulsed primary ion beam to desorb and ionize species from a sample surface. The resulting secondary ions are accelerated into a mass spectrometer, where they are mass analyzed by measuring their time-of-flight from the sample surface to the detector. ToF-SIMS mass spectra can be used for determination of the elemental and molecular species on a surface (mass spectra); visualization the distribution of individual species on the surface (by imaging); and to determine the distribution of different chemical species as a function of depth from the surface (depth profiling). The sampling depth of ToF-SIMS is in the range of 1–2 nm and the lateral resolution for the imaging ~200 nm. In comparison with XPS, ToF-SIMS provides more chemical structural information. However, the surface topographic and contamination effects due to high surface sensitivity often make the interpretation of the mass spectra complicated for unknown samples.

The application of ToF-SIMS in the study of fiber, wood and paper surfaces has been reported by many authors (Detter-Hoskin 1995, Brinen 1993, Pachuta 1994, Fardim 2005a, b, Tokareva 2011, Bryne 2008, Kangas 2007). ToF-SIMS provides qualitative information on the chemical structure of carbohydrates, lignin and extractives and their lateral distributions in the outermost surface layer of pulp. ToF-SIMS imaging was found a valuable chemical microscopy technique for paper and paper coatings, and to assess the spatial distribution of components in wood tissues. ToF-SIMS has also been utilized to study the chemical interaction between silane film and metal substrates (Bexell 2003, Fedel 2010).

# 4. MATERIALS AND METHODS

## 4.1 TMP fibers and characterization

***TMP fibers and chemical treatments***

The analyzed TMP fibers were latewood-enriched, i.e. thick-walled, long fibers separated from 1st stage Norway spruce TMP (*Picea abies*). The TMP was produced in pilot scale (KCL, Oy Keskuslaboratorio – Centrallaboratorium Ab, Espoo) in a single disc refiner (B1, 44") with 1500 rpm, 450 kPa and specific energy consumption of 1.2 MWh/t. The 1st stage TMP was screened in a two-stage slot screen (0.15 mm) to remove shives and then dewatered on a disk filter. The latewood enrichment was executed by a special mobile Noss hydrocyclone treatment at a low inlet consistency of 0.14%. Heavy thick-walled latewood fibers as well as unfibrillated fibers having a low specific surface area tend to move towards the reject stream in the hydrocyclone and thus leave through the apex from where they were collected for further investigation. The long fibers were separated from this material by Bauer-McNett cascade fractionation according to standard SCAN method (SCAN-M6). The +14 mesh and 14/28 mesh fractions were mixed. The latewood content of this material was 42% measured by microscopy with the method recommended by Mork (Mork 1928). Selected properties of the long fibers are given in Table 1.

**Table 1.** Characteristics of the 1st stage TMP from which the studied long fibers were separated for chemical treatments.

| | *1st stage TMP* |
|---|---|
| Canadian Standard Freeness (CSF), ml | 760 |
| Length-weighted fiber length (FS200), mm | 2.12 |
| Dynamic Drainage Jar (DDJ)-fines content, % | 1.7 |
| Fiber wall thickness (light microscope), µm | 5.21 (0.18)[1] |
| Fiber width (light microscope), µm | 35.48 (0.90)[1] |
| Cell-wall index CWI[2] | 0.294 |

[1] 95% confidence interval is given in the brackets

[2] CWI = (2 x Fiber wall thickness) / Fiber width

The long fibers were treated either with sodium oxalate solution buffered with oxalic acid dihydrate (hereafter called as buffered sodium oxalate, OX) or with hydrochloric acid (AC). The pH value of both solutions was approximately 2.5. Reference treatment (REF) was performed with deionized water at pH 6. The conditions for all the treatments are

given in Table 2. In all cases, fiber consistency was 2% and the treatment temperature 130ºC. All mechanical treatments, such as mixing and stirring, were the same for all trials.

**Table 2.** Fiber treatment conditions.

| *Sample name* | *Treatment* | *Amount of chemical on o.d. fiber (mmol/g)* | *Initial pH* | *Treatment time (min)* | *Total contact time (min)* |
|---|---|---|---|---|---|
| REF | De-ionized water | | 6.0 | 15 | 53 |
| OX | Na-oxalate buffered with oxalic acid dihydrate | 6.0 | 2.6 | 15 | 49 |
| AC | HCl | 1.14 | 2.5 | 15 | 51 |

***Fiber characterization***

A special single fiber analysis procedure for inspection with different microscopy techniques was developed. This technique enabled the imaging of the same specific fiber with all the microscopy methods. The principle is depicted in Figure 3.

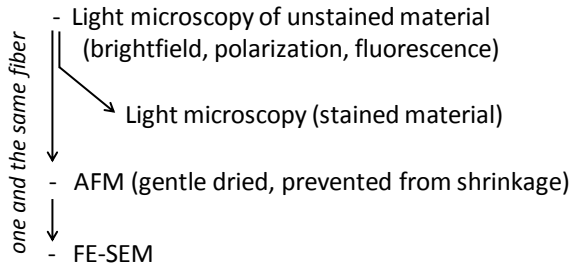


**Figure 3.** Single fiber inspection sequence with light microscopy, AFM and FE-SEM.

Moist fibers with visible bands of intact outer fiber wall were selected under the light microscope. The fibers were placed and aligned in parallel onto a circular glass plate of 15 mm diameter. The fiber ends were fixed with water-proof tape, and the glass plate was then brought to an object slide fixed with a drop of water-glycerin. A drop of water was

applied onto the fibers. Finally, the fibers were covered with a cover slide and kept in a cool and dark storage room. For AFM measurements, dry fibers are preferred. The fibers fixed on the glass plates and covered with standard cover glass were permitted to dry gently in the storage room at 8ºC. Before AFM imaging, the cover glass was carefully removed. By this procedure, minor changes in the surface structure cannot be avoided, and some shrinkage was observed. These minor changes are assumed not to affect the comparison of the samples, since the same preparation procedure was applied to all samples. After AFM measurement, the same glass plates with fibers fixed on them were studied by FE-SEM. The glass plates were mounted to the sample holder and the fibers were sputtered directly on the glass support.

As shown in Figure 3, each single unstained fiber was first inspected in a light microscope applying bright field, polarization, surface scatter and combinations of these optical techniques. These illumination modes were applied to visualize distinctive parts of the fiber wall – bands of intact outer (ML/P) fiber wall, and exposed areas of inner ($S_2$) fiber wall. Additionally, selected fibers were stained with Rhodamine Red and Toluidine Blue to further improve the visibility of morphologically different fiber wall areas. Images were taken from all inspected single fibers. The positions of the different fiber wall parts were marked to localize them again when analyzing the fibers by AFM and FE-SEM. At least five fibers of each sample type were analyzed.

The AFM measurements were carried out at ambient conditions with a Nanoscope IIIa (Digital Instruments Veeco Meterology Group, Santa Barbara, CA) instrument. The microscope was placed on an active vibration isolation table (MOD-1, JAS Scientific Instruments), which was itself placed on a massive stone table to eliminate external vibration noise. All images were obtained with a J-scanner in tapping mode and using silicon cantilevers (NSC15/NoAl, μmasch$^{TM}$) with a radius of curvature of the tips less than 10 nm. The free vibration amplitude of the cantilever was 80 ± 5 nm, and a damping ratio (tapping amplitude/free amplitude) within 0.60–0.75 was used for imaging. Topographical and phase images were recorded simultaneously using a scan speed of 0.8–1 Hz with a pixel resolution of 512 × 512. The image size was 3 μm × 3 μm. On average 9 images, varying from 4 to 12, were measured for both inner and outer fiber wall areas in order to obtain statistically representative data. RMS roughness, kurtosis and skewness, calculated with the commercial SPIP-software (Image Metrology A/S, Denmark), were used for characterization of surface differences between the outer and the inner fiber wall areas.

The morphology of pulp fibers was also imaged using a Field Emission Scanning Electron Microscope (FE-SEM, Jeol JSM 6335F). A low acceleration voltage (1 kV) was used. Fibers were sputter-coated with a thin layer of Au-Pd. The same areas as already studied with the light microscope and measured by AFM were localized in FE-SEM.

## 4.2 Modification and characterization of wood and paper

***Wood and paper substrates and sol-gel coatings***

The wood substrate materials in Paper II were sawn timber from pine sapwood (*Pinus sylvestris)* and heat-treated spruce (*Picea abies*). The sample size was 100 mm × 50 mm × 5 mm (longitudinal × tangential × radial for pine and longitudinal × radial × tangential for spruce). Samples with the dimensions of 10 mm × 10 mm × 5 mm were cut from the original samples and subjected to AFM and ToF-SIMS analyses. Half of the original samples (50 mm × 50 mm × 5 mm) were used for contact angle measurements. The heat-treated spruce was Thermo-S (S stands for Stability) produced according to a methodology developed by VTT (Viitaniemi 1994). All the wood specimens were preconditioned at 50% of relative humidity (RH) and 20ºC prior to the sol-gel modification.

The wood and paper substrates in Papers III-V were base paper (43 g/m$^2$, moisture content 8.3%, from unbleached softwood chemical pulp, Paper III), industrial phenolic resin (PF) impregnated paper (120 g/m$^2$, delivered by Stora Enso Laminating Paper Oy, Kotka, Finland, Paper IV) and birch plywood (Paper V). Industrial impregnated paper is normally pre-cured at 160ºC for 20–25 s.

Three silane-based sol-gel coatings (coating A, B, C) were developed by VTT and used in Papers II-V in order to modify surface energy and control the moisture behavior of the studied wood and paper. Coatings A and B are fluorine free coatings, which differed from each other in terms of the length of the organic aliphatic chain. The alkoxysilane in coating A is methyltriethoxysilane (MTEOS) and in coating B octyltriethoxysilane (OTEOS). Coatings A and B were either spread onto the tangential pine and the radial heat-treated spruce surfaces (Paper II) using a brush or spray coated into base paper (Paper III) and industrially PF impregnated paper (Paper IV). Coating C contains a fluorocarbon group ($CF_3$–) attached to the silane backbone (fluorocarbon-containing triethoxysilane (FTEOS)). The sol-gel coatings B and C and phenolic resin were used in Paper V for the paper modification. The modified paper was further pressed onto plywood at 135ºC, 18 bar, for 5 minutes. In this thesis, the sol-gel coatings are labeled as MTEOS, OTEOS, FTEOS, corresponding to labels coating A, B, C used in Papers I-V.

Spray coating of sol-gels to paper was performed with a Spray-combo device developed by VTT in Jyväskylä, Finland using different amounts of sol-gel measured by dry basis weight. The solids content of the coating was optimized to 15 wt%. The desired amount of coating was applied by varying the amount of coating layers (1–5) and non-volatile content, followed by blow drying and a separate heat treatment (thermal curing) of coated papers.

The wet spreading amounts of the coatings for pine sapwood and heat-treated spruce were 100–120 g/m$^2$. In papers III-IV, the same spraying amount was applied to base paper and PF impregnated paper with a thermal curing at 110ºC for 1 hour. As a reference treatment, paper was sprayed with water (same amount as used for preparing the coatings) followed by a thermal heating at 110ºC for 1h. In paper V, the OTEOS and FTEOS sol-gel coatings were also applied by spray coating to the paper substrates. The details can be found in Table 3.

**Table 3.** Paper samples treated with OTEOS and FTEOS.

| *Paper samples* | *Treatment* | *Treatment conditions* |
|---|---|---|
| Base paper + OTEOS | Base paper was surface treated with OTEOS (coating amount 1.3 g/m$^2$, dry weight) | The coating was cured in the oven at 110ºC for 15 minutes |
| Base paper + FTEOS | Base paper was surface treated with FTEOS (coating amount 0.8 g/m$^2$, dry weight) | The coating was cured in the oven at 110ºC for 15 minutes |
| Industrially impregnated paper + OTEOS | Industrially impregnated paper was surface treated with OTEOS (coating amount 1.1 g/m$^2$, dry weight) | The coating was cured in the oven at 110ºC for 15 minutes |
| Industrially impregnated paper + FTEOS | Industrially impregnated paper was surface treated with FTEOS (coating amount 1.6 g/m$^2$, dry weight) | The coating was cured in the oven at 110ºC for 15 minutes |

***Surface analysis***

The morphology of sol-gel coated wood and paper was examined by SEM (Paper III-IV), AFM (Paper II-V) and CLSM (Paper III-IV). XPS and ToF-SIMS were used to examine the surface chemical composition of studied wood and paper samples (Paper II-V). ToF-SIMS was mainly used to examine the distribution of sol-gel coatings on the surfaces of modified wood and paper. In addition, ATR-FTIR was performed to probe the possible chemical bonds between the sol-gel coating and impregnated paper (Paper III). The wettability of wood and paper was evaluated by contact angle measurements (Paper II-IV) and surface energy determination (Paper IV). The contact angles were determined by the

sessile drop method, where a liquid droplet was deposited on the solid surface and the contact angle was determined in time. A modified Cobb method (ISO 535) was used to evaluate the water absorption of film-coated plywood (Paper V). More details about the surface analysis can be found in Papers II-V.

# 5. RESULTS AND DISCUSSION

This chapter contains a summary of the main results from Papers I-V. In section 5.1, the effects of chemical treatments on micro and nano-scale surface structure of 1st stage TMP latewood fibers from Norway spruce are discussed (Paper I). Sections 5.2 and 5.3 discuss the surface and wetting properties of pine sapwood, heat-treated spruce and paper substrates modified with sol-gel coatings (Paper II-IV). Section 5.4 summarizes the results from the laminated plywood (Paper V).

## 5.1 Characterization of TMP fiber wall surface structure

In this section, the effect of buffered sodium oxalate (OX) and hydrochloric acid (AC) on fiber wall surface structure of TMP fibers is discussed. In this case, the outer as well as the inner fiber wall layers of the untreated and chemically treated fibers were separately analyzed by LM, AFM and FE-SEM.

The results show that the inner ($S_2$) and outer (M/P) layers can be clearly distinguished by light microscopy with various optics. The outer layer appears as bands around the fiber, and the inner layer can be seen as swollen areas (Figure 4). In order to find out the effect of chemical treatments, the outer and inner layers were further investigated with AFM and FE-SEM. The representative AFM phase images (Figure 5) reveal that the inner and outer fiber walls of the reference pulp (REF) can clearly be distinguished due to their different visual appearance and roughness. The outer layer is rougher than the inner layer due to the different structural properties of the outer and inner wall layers. When fibers were treated with OX, the inner layer appears similar to that of REF. The outer layer is however rougher than the one for REF. With respect to the effect of hydrochloric acid on the inner layer and outer layer, the AC treatments cause some granular structures in the inner layer which can be interpreted to be lignin. In addition, the inner layer for AC fiber is clearly rougher than that of the REF fiber and slightly rougher than that of the OX fiber. This is probably partly due to the presence of the granules. However, the average surface roughness values calculated from nine images from each type of wall area (Figures 6-8) indicate that the different chemical treatments do not cause significant differences in the mean *Sq* roughness values of the inner layers. However, OX results in the highest surface roughness in the outer layer and causes the largest difference between the outer and the inner wall roughness. As can be seen from the $S_{ku}$ values (Figure 7), the AC causes the largest change in the surface peak distribution of the inner wall areas. The largest difference in kurtosis between the inner and the outer fiber wall areas is found in AC-treated samples. No visible changes are introduced to the surface height distribution of the outer fiber wall areas by any of the chemical treatments. Surface porosity of inner and outer layers was evaluated by the skewness, $S_{sk}$, shown in Figure 8. The AC

treatment creates most surface pores in the inner wall areas. Similar, but lower tendency is seen for the inner fiber wall areas of the OX treated fibers. The surface pores can be ascribed to the dissolved hemicelluloses by AC or OX treatments. The outer layer surfaces appear to be less porous than the corresponding inner layers, especially in the REF sample. This is assumed to be due to the high lignin and low hemicellulose content of the outer fiber walls, which decreases the possibility for removal of hemicellulose by hydrolysis.

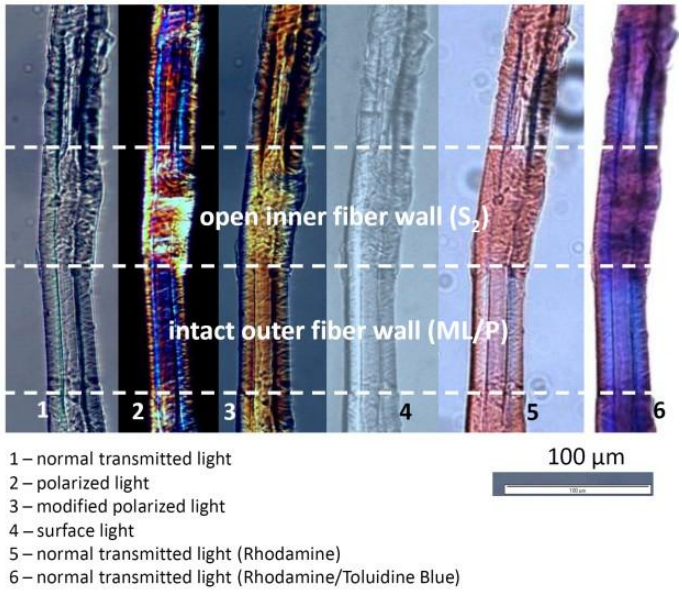


**Figure 4.** Intact outer (M/P) fiber wall areas and exposed inner ($S_2$) fiber wall area along fiber length axis revealed by different light microscopy techniques.

**a) REF samples**


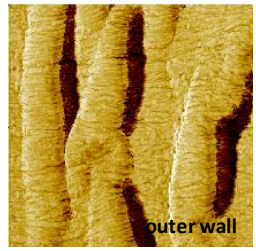


| Fibril angle, ° | 20 | 87 |
|---|---|---|
| $S_q$, nm | 14.2 | 45.3 |
| $S_{ku}$ | 4.49 | 2.28 |
| $S_{sk}$ | 0.26 | 0.10 |

**b) OX samples**



| Fibril angle, ° | 12 | 69 |
|---|---|---|
| $S_q$, nm | 21.6 | 54.4 |
| $S_{ku}$ | 3.96 | 2.69 |
| $S_{sk}$ | -0.41 | -0.07 |

**c) AC samples**

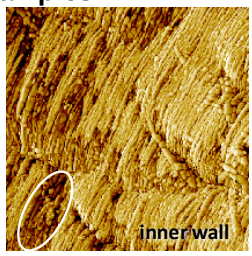



| Fibril angle, ° | 25 | 76 |
|---|---|---|
| $S_q$, nm | 23.6 | 26.7 |
| $S_{ku}$ | 4.38 | 2.91 |
| $S_{sk}$ | -0.78 | 0.13 |

**Figure 5.** AFM phase images, fibril angle and surface roughness parameters of reference fiber (REF), fiber treated with buffered sodium oxalate (OX) and fiber treated with hydrochloric acid (AC). The images are 3 μm x 3 μm.

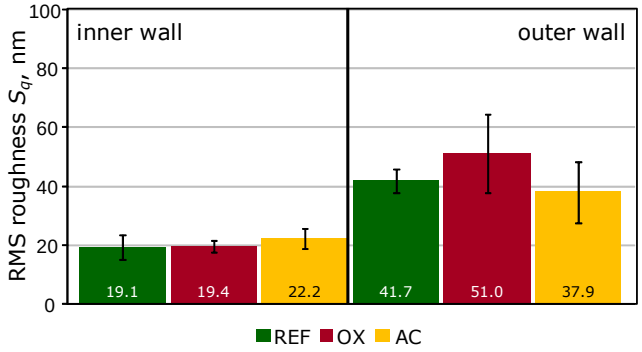


**Figure 6.** RMS roughness $S_q$ of inner and outer fiber wall parts.

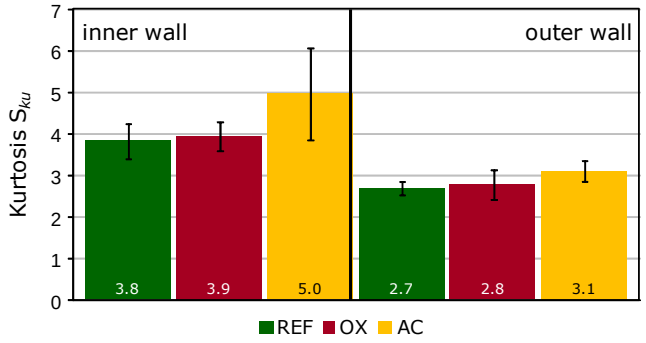


**Figure 7.** Kurtosis $S_{ku}$ of inner and outer fiber wall parts.

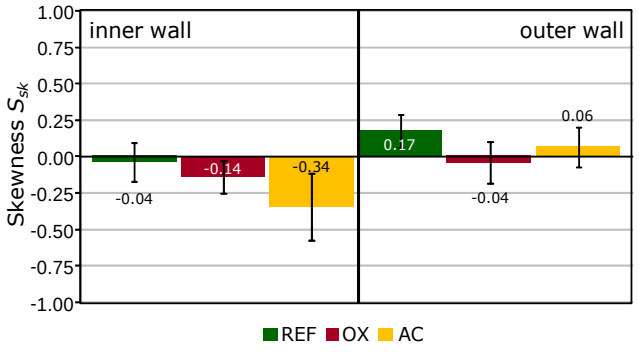


**Figure 8.** Skewness $S_{sk}$ of inner and outer fiber wall parts.

The same single fibers, which were measured by AFM, were also studied by FE-SEM to compare the information obtained with these two techniques. As shown in Figure 9, for visual characterization of the fiber surface structures, FE-SEM can give high-quality information comparable to AFM.

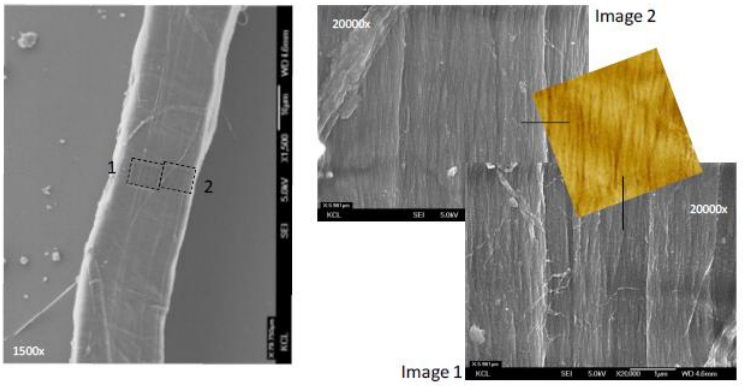


**Figure 9.** FE-SEM images of the inner ($S_2$) fiber wall surface of the reference sample (REF). The small colored image is a corresponding AFM image (3 μm x 3 μm). The scale bar in image 1 is 1 μm.

### 5.2 Surface characteristics of sol-gel coated pine sapwood and heat treated spruce

The effects of the two alkoxysilane sol-gel coatings (MTEOS and OTEOS) on surface properties and moisture behavior of pine sapwood and heat-treated spruce were studied by AFM, XPS, ToF-SIMS and water contact angle measurements (Paper II). The results are briefly discussed below.

***Surface morphology***

The surface morphology of uncoated and coated pine sapwood and heat-treated spruce at micro-scale were determined by AFM. As apparent in Figure 10, the deposited sol-gel coatings appear as particulate and/or film-like structures. MTEOS appears as a more even layer than OTEOS. In order to estimate the coating-induced changes in smoothness, the surface RMS roughness ($S_q$, Figure 11) values of pine sapwood and heat-treated spruce were calculated from at least 8 topographical images. It is seen that MTEOS has a stronger tendency than OTEOS to smoothen the wood surfaces at the studied micro-scale. In addition, the level of roughness of the coated samples is relatively the same independent of the substrate (wood species). The SEM-EDS imaging of coated wood cross-sections suggests that MTEOS likely deposits more on the surface and in the upper layers and therefore smoothens the substrate surface structure (Appendix I). However, more images are required to statistically confirm this observation.

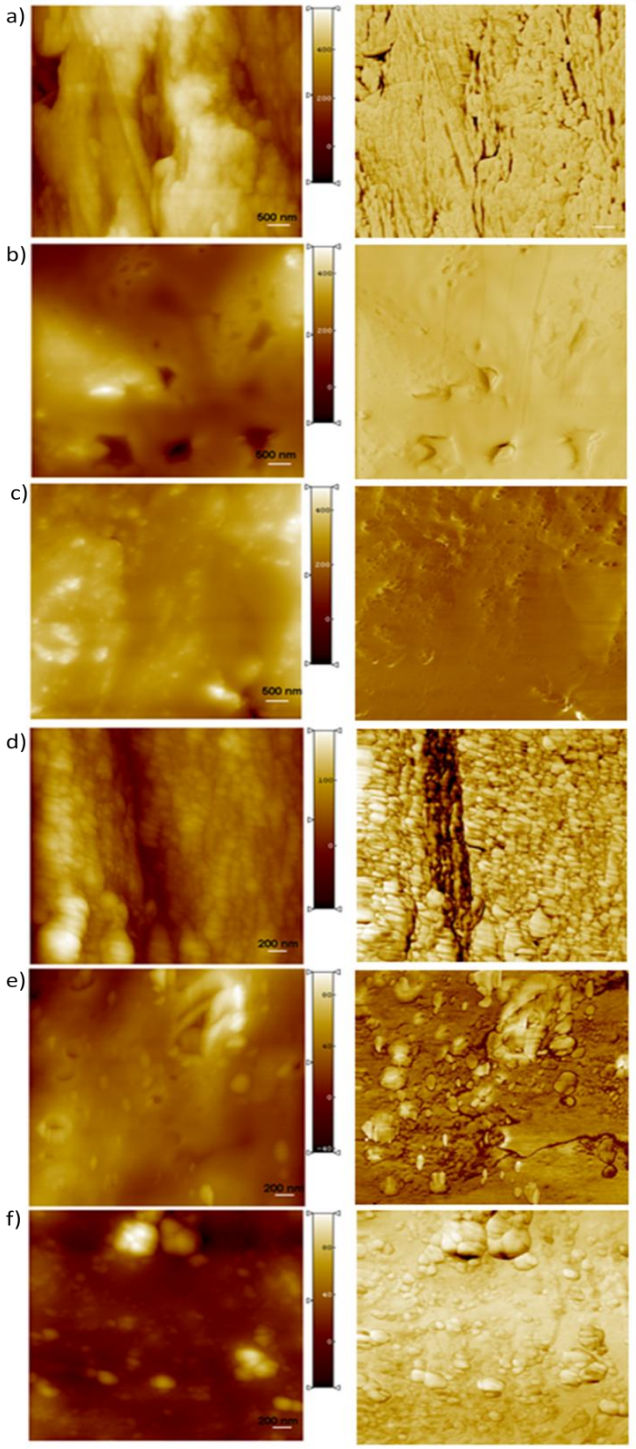


**Figure 10.** Representative AFM topographical and phase images of a) pine sapwood b) pine sapwood with MTEOS, c) pine sapwood with OTEOS, d) heat-treated spruce, e)

heat-treated spruce with MTEOS, and f) heat-treated spruce with OTEOS. The image size is 6 µm × 6 µm for pine sapwood and 3 µm × 3 µm for heat-treated spruce. The scale bar is 500 nm in images a-c and 200 nm in images d-f.

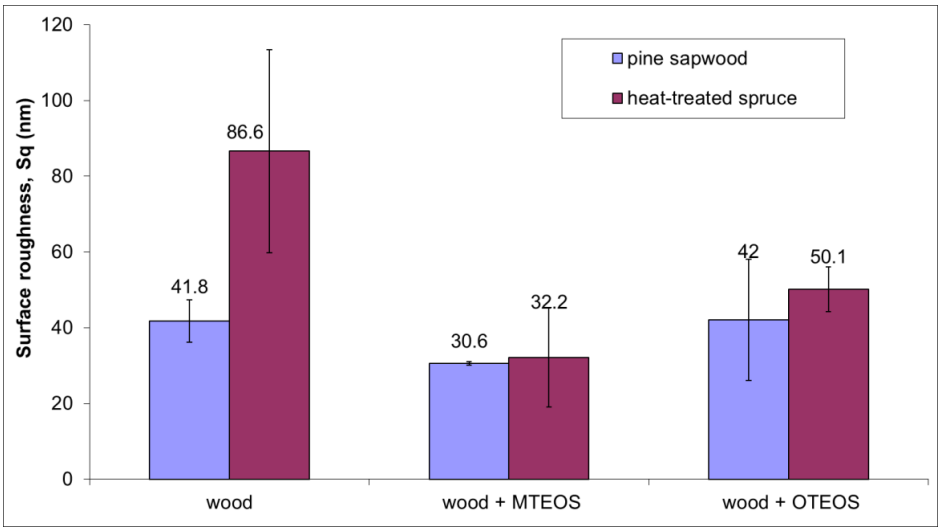


**Figure 11.** Surface RMS roughness, $S_q$, of pine sapwood and heat-treated spruce before and after modification with MTEOS and OTEOS. The AFM image size is 3 µm x 3 µm.

***Surface chemistry***

Surface composition of the wood samples was studied by XPS using both survey and high resolution spectra. Previous research verified the chemical covalent bonds between the sol-gel coating and the wooden surface by ATR-FTIR and XPS (Tshabalala 2003a). The elemental composition from survey spectra and the concentrations of C1–C4 components from C1s high resolution spectra are summarized in Table 4. C1 corresponds to carbon linked to hydrogen or carbon (–C–H or –C–C), C2 to carbon linked to one oxygen (–C–O), C3 to carbon linked to two non-carbonyl oxygen atoms (–O–C–O–), or one carbonyl oxygen (–C=O), and C4 to carbon linked to carbonyl and non-carbonyl oxygen (O=C–O–).The elemental composition data indicates a successful deposition of the sol-gel coatings. The silicon content of the coated specimens is approximately 18% (MTEOS) and 14% (OTEOS) whereas practically no silicon is observed on the uncoated pine sapwood. The corresponding silicon amounts are approximately 12% (MTEOS) and 13% (MTEOS) for heat-treated spruce. The carbon content of the coated specimens decreases approximately 42% (MTEOS) and 30% (OTEOS) for pine sapwood and approximately 29% (MTEOS) and 34% (coating B) for heat-treated spruce. On the other hand, the oxygen content increases approximately 24% (MTEOS) and 14% (OTEOS) for pine sapwood, and approximately 16% (MTEOS) and 20% (OTEOS) for heat-treated spruce. The increase in the surface oxygen content and decrease in the surface carbon

content suggests that the coated wood surfaces are completely covered by the sol-gel coatings. The typical thickness of the deposited sol-gel coatings was ~1–2 μm, whereas the depth resolution of XPS is about 5–10 nm, therefore, it is only the composition of sol-gel coatings which is measured by XPS. It is also interesting to note that OTEOS results in similar surface chemistry for pine sapwood and heat-treated spruce. However, MTEOS absorbs more into the surface of pine sapwood than onto the surface of heat-treated spruce. It is known that the main components of wood (cellulose, hemicelluloses, and lignin) degrade in different ways under heat. Cellulose and lignin degrade more slowly and at higher temperatures than the hemicelluloses. The extractives in wood degrade more easily, and these compounds evaporate from wood during the heat treatment. For example, migration of wood resins onto the surface of wood has been observed at low temperatures 100–160°C; the lipophilic compounds in wood, such as fats, waxes, and steryl esters, migrate to the surface of wood after heat treatment and form a monolayer or a structured multilayer. In general, a rise in temperature from 180 to 225°C (temperature used in heat treatment process) results in a steady increase of the mass fraction of lignin with a simultaneous decrease of the carbohydrate content (Alén 2002). Therefore, in principle, there are less hydroxyl groups on heat-treated spruce surface than on pine sapwood accessible to the hydrogen bonding with the applied sol-gel coatings. It is reasonable to conclude that with the same coating amount, less coating will be covalently bound onto heat treated spruce surface.

Regarding the chemical bonds, both coatings led to a decrease of the C2–C4 components. The increase of C1 component for all the sol-gel coated samples is evidence of the presence of C–C and C–H structures arising from the hydrocarbon chains of the coatings. This is in agreement with Tshabalala's study which ascribed the increase of the C1 component to the hydrocarbon chains in the coatings.

**Table 4.** Surface chemistry of uncoated and coated pine sapwood and heat-treated spruce by XPS.

| *Samples* | *C* | *O* | *Si* | *C1 (%)* | *C2 (%)* | *C3 (%)* | *C4 (%)* |
|---|---|---|---|---|---|---|---|
| Pine sapwood | 74.0 | 26.0 | <0.1 | 60.9 | 26.0 | 7.1 | 5.9 |
| Pine sapwood + MTEOS | 32.3 | 49.7 | 18.0 | 77.8 | 12.7 | 4.0 | 5.5 |
| Pine sapwood + OTEOS | 44.8 | 40.8 | 14.5 | 85.6 | 12.2 | 1.9 | 1.4 |
| Heat-treated spruce | 79.4 | 20.6 | <0.1 | 69.6 | 23.6 | 4.0 | 2.8 |
| Heat-treated spruce + MTEOS | 50.8 | 36.7 | 12.5 | 81.3 | 15.2 | 1.3 | 2.3 |
| Heat-treated spruce + OTEOS | 45.5 | 40.6 | 13.5 | 82.7 | 12.9 | 2.5 | 1.9 |

***Distribution of sol-gel coatings on wood surfaces***

The distribution of the applied sol-gel coatings on pine sapwood and heat-treated spruce is shown in Figure 12. The light-dark contrast in the images represents high-low ion intensity. The sol-gel coatings are spread fully on the pine sapwood surfaces with a slightly higher deposition onto the cell walls. For heat-treated spruce, both coatings deposit on the sample surface with a high concentration of MTEOS around the pit edges (Figure 12d). Thin coatings are presumably formed since the original wood texture is visible. Moreover, less coating is found on the fiber macro-voids of heat-treated spruce than on the pine sapwood. This observation is reasonable since the surface of heat-treated spruce is much rougher and less polar than pine sapwood (Figure 11, Table 4), which suggests weaker adhesion of the coating to the heat-treated spruce than to the pine sapwood.

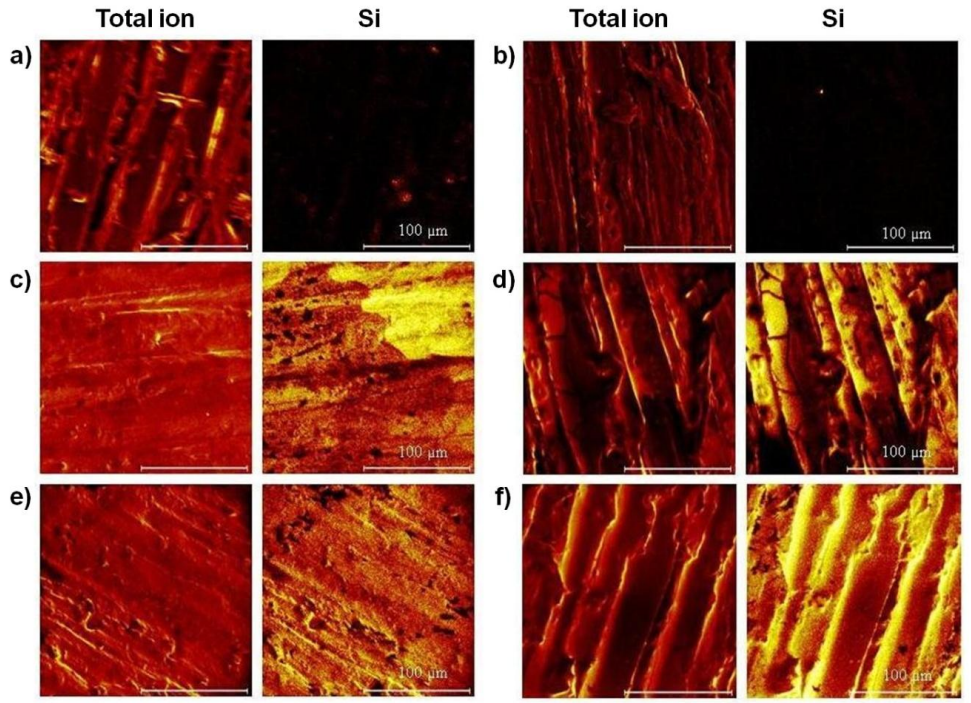


**Figure 12.** Total positive and $Si^{4+}$ ion distribution on (a) pine sapwood, (c) pine sapwood with MTEOS, (e) pine sapwood with OTEOS, (b) heat-treated spruce, (d) heat-treated spruce with MTEOS and (f) heat-treated spruce with OTEOS.

***Water repellency***

The effect of sol-gel coatings on water repellency of pine sapwood and heat-treated spruce was studied by water contact angle measurements. The results obtained from contact angle measurements (Figure 13) indicate that both sol-gel coatings resulted in rather similar contact angles irrespective of the coated substrate: immediately after stabilization on the surfaces, the initial contact angle values on the two wood materials were ~80° for MTEOS and ~105° for OTEOS coating. In addition, monitoring of the droplet volumes throughout the contact angle measurements indicated that OTEOS results in an impermeable surface for both pine sapwood and heat-treated spruce. MTEOS leads to a permeable surface for pine sapwood, but an impermeable one for heat-treated spruce. Thus, OTEOS performs as a better barrier for pine sapwood and heat-treated spruce than MTEOS. In addition, one should note that the reference heat-treated spruce is slightly more hydrophobic than the reference pine sapwood. It has been reported earlier that drying wood at high temperatures lowers the surface wettability, partly due to the migration of wood extractives to the surface (Nuopponen 2003). The higher contact angle for untreated heat-treated spruce may be due to different factors: (1) the hydrophobic nature of heat-treated spruce, (2) presence of adequate fine (nano-scale)

surface features on the heat-treated spruce samples (as a result higher roughness values compared to the pine surfaces were recorded), or (3) both of these factors. Water uptake of wood is known to be slower in the radial direction compared to the tangential or longitudinal directions (Derome 2005), and thus, the water permeability of the tangential pine and the radial heat-treated spruce surfaces are expected to differ from each other. In addition, the bordered pits in spruce are known to be mainly at the aspirated state which limits water transfer through the pit openings. On the other hand, thermal treatment changes the porosity and density of wood and can make the wood surfaces more permeable compared to the untreated material (Pfriem 2009). However, with Norway spruce drastic damages due to thermal treatments, e.g. detachment of cells or cell wall layers, or destruction of pits through degradation of pit membranes have not been observed (Boonstra 2006).

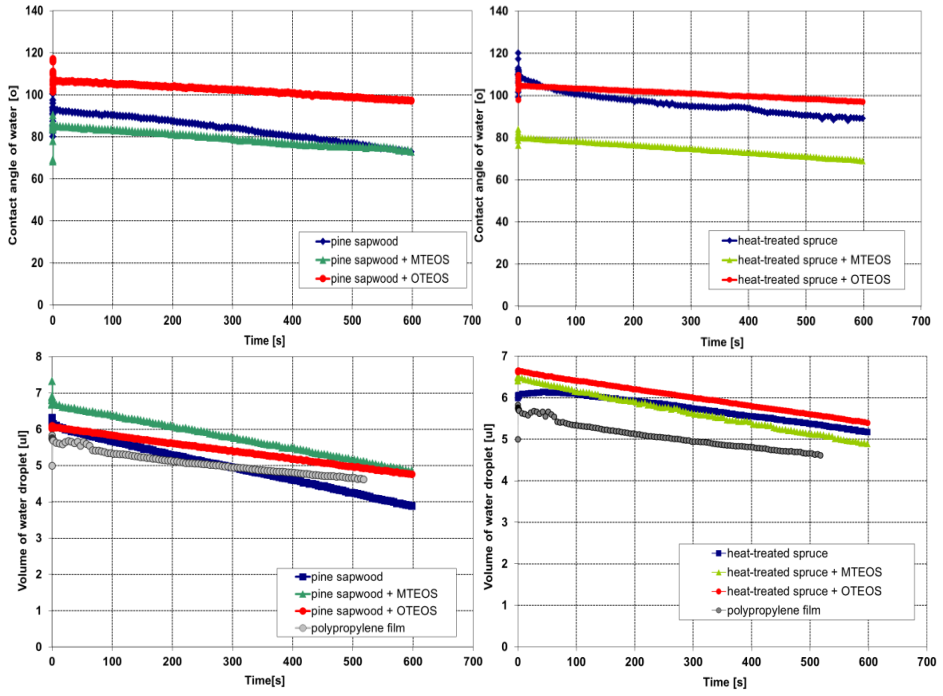


**Figure 13.** The water contact angle measurements for the uncoated and the coated pine sapwood, and the heat-treated spruce. The polypropylene film was used as a non-penetrating reference surface.

### 5.3 Surface characteristics of spray coated base paper and impregnated paper

***Surface morphology***

The sol-gel coatings (MTEOS and OTEOS) used above for wood surface modification were also used to spray coat the base paper and PF impregnated paper (Papers III-IV). A

water treatment was used as a reference to evaluate the effect of curing process of the coatings on the surface properties.

The surface morphology of base paper and PF impregnated paper before and after different treatments was studied by CLSM, SEM and AFM. The CLSM and SEM images were used to investigate the surface morphology at macro-scale, while AFM images gave more structural details at micro-scale. In Figure 14, the CLSM images reveal that the structure of water-treated as well as MTEOS coated base paper appears rather similar to the reference base paper and PF impregnated paper. Similarly no clear visual difference between the surfaces of the OTEOS coated base paper and the reference base paper can be observed. Nevertheless, the surface of OTEOS coated impregnated paper appears to differ from the other samples. The fibers under the coating are no longer visible. This sample consists of large continuous and smooth areas which are separated by cracks. In order to gain more information of the surface morphology, SEM images were analyzed (Figures 15 & 16). It can be seen that the structure of water-treated base paper appears rather similar to that of the reference. MTEOS together with OTEOS appears as smooth films on the fiber surfaces of base paper and partially fills the intersections of the neighboring fibers. For the PF impregnated paper, the water treatment causes a more continuous surface with partially exposed fiber structures. This is because the industrially impregnated paper is partially cured; consequently, the structural change may have been caused by the further curing of the PF resin in the paper during the heat treatment. The surface morphology of the impregnated paper with MTEOS resembles that of the untreated impregnated paper with the same kind of structural boundaries (cracks) and local defects which are possibly due to bubbles or local de-wetting. In addition, local cracks induced by the coating are observed. In comparison with MTEOS, OTEOS results in larger continuous and smooth areas on the impregnated paper in spite of the local defects and cracks after the treatment. A further study of the deposited film morphology at micro-scale was carried out by AFM. As shown in Figure 17, it is evident that the deposited sol-gel films on base paper surfaces are virtually discontinuous. Both coatings appear to behave differently on the surfaces of industrially impregnated paper; in particular, particle-like structures can be observed on the surface of OTEOS coated paper (Figure 17g and h).

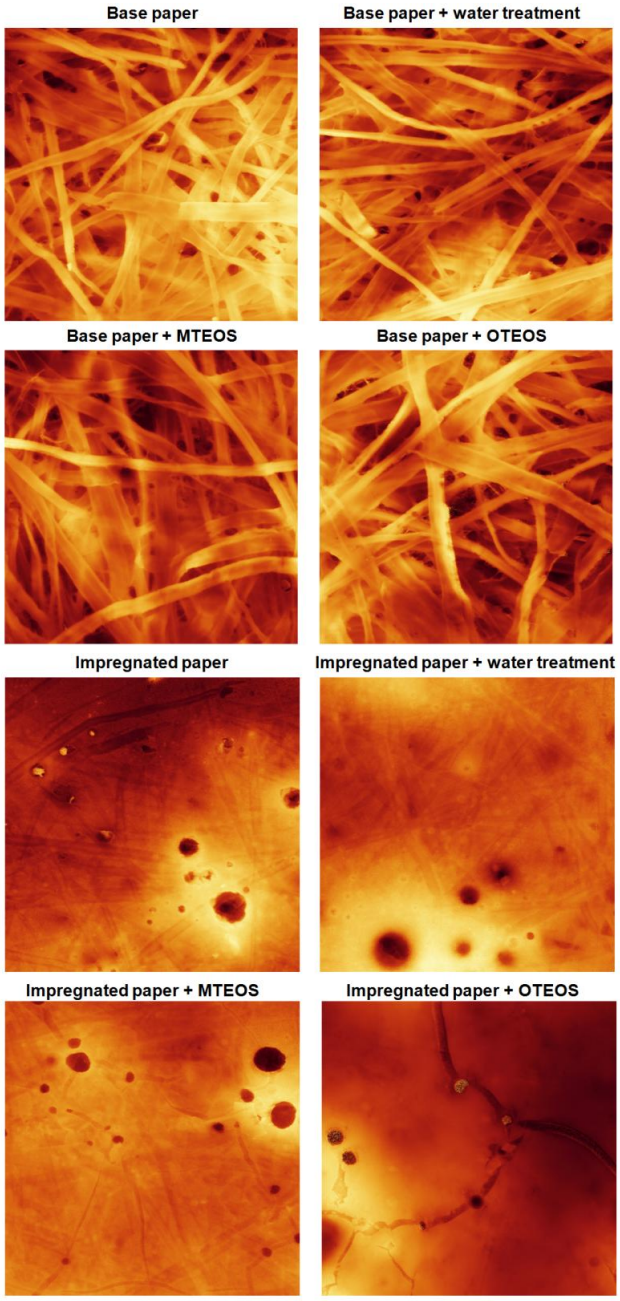


**Figure 14.** CLSM images of reference paper, treated base paper and PF impregnated paper. The image size is 1.5 mm x 1.5 mm.

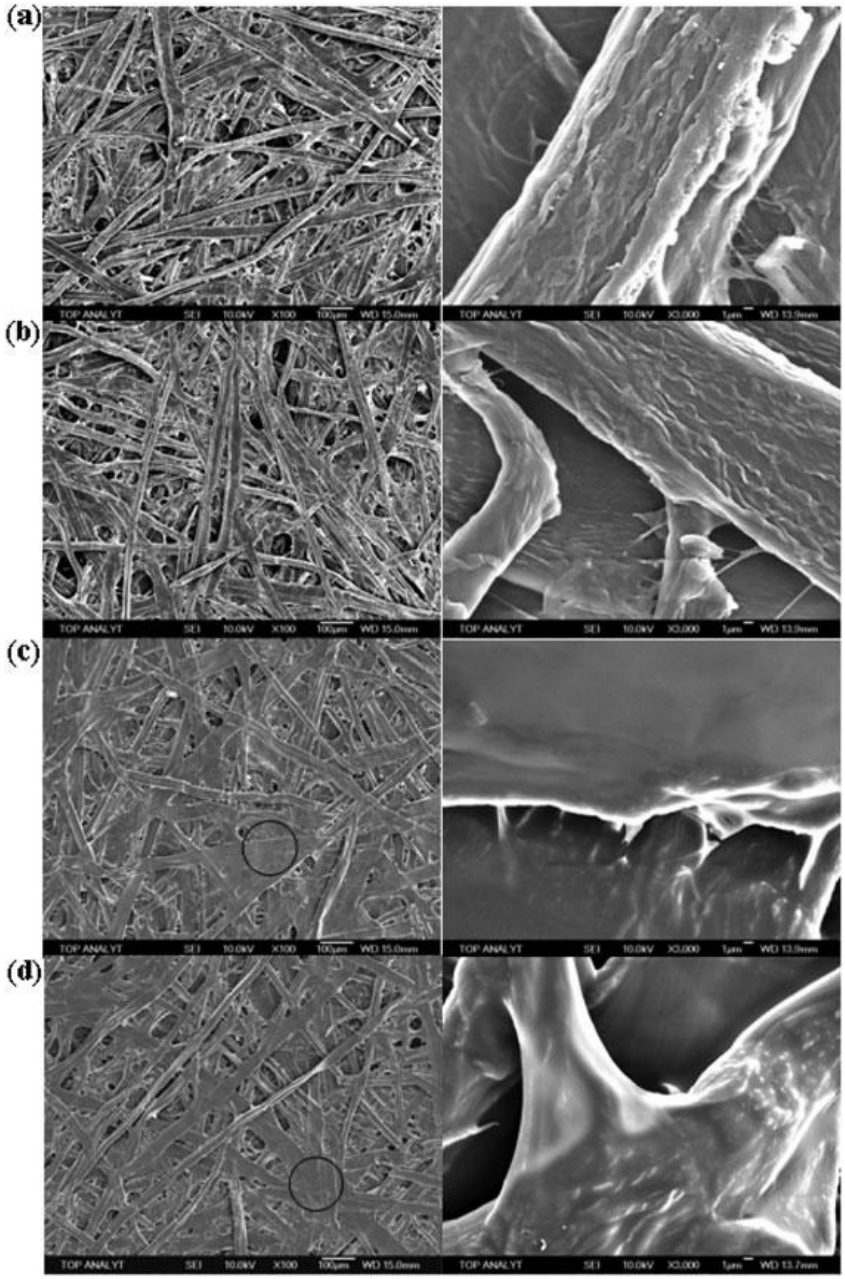


**Figure 15.** SEM micrographs of the surfaces of (a) base paper, (b) base paper with water treatment, (c) base paper with MTEOS, and (d) base paper with OTEOS. The scale bar is 100 μm and 1 μm, respectively. The areas marked with a circle indicate intersections of neighboring fibers being partially filled by the applied coatings.

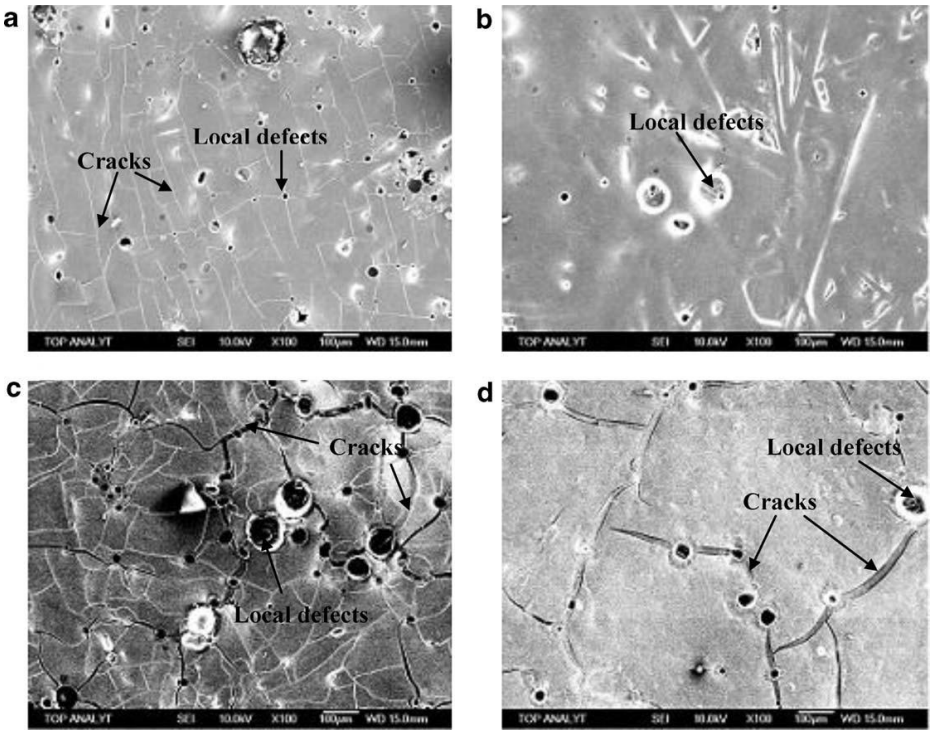


**Figure 16.** SEM micrographs of the surfaces of (a) impregnated paper, (b) impregnated paper with water treatment; (c) impregnated paper with MTEOS, and (d) impregnated paper with OTEOS. The scale bar is 100 μm.

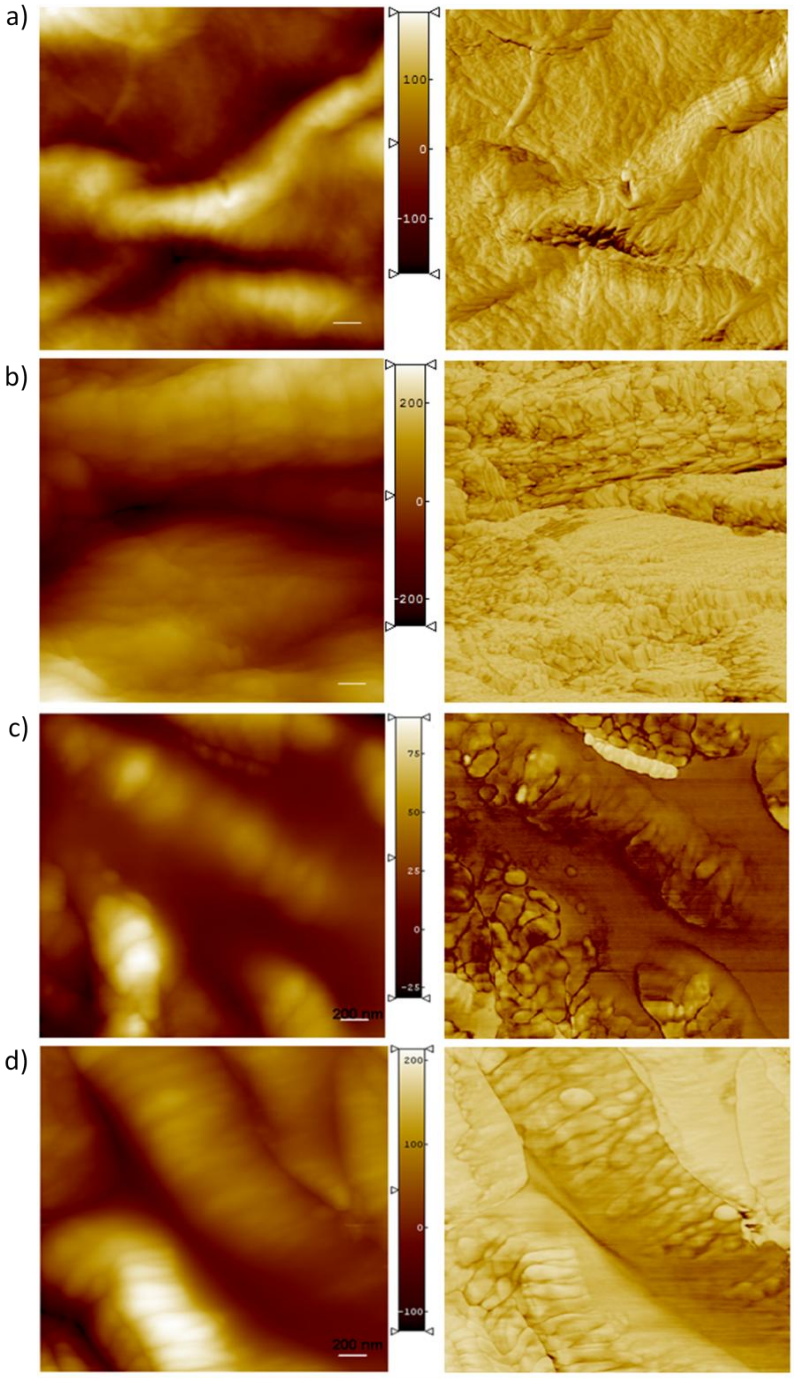
a)
100
0
-100
b)
200
0
-200
c)
75
50
25
0
-25
200 nm
d)
200
100
0
-100
200 nm

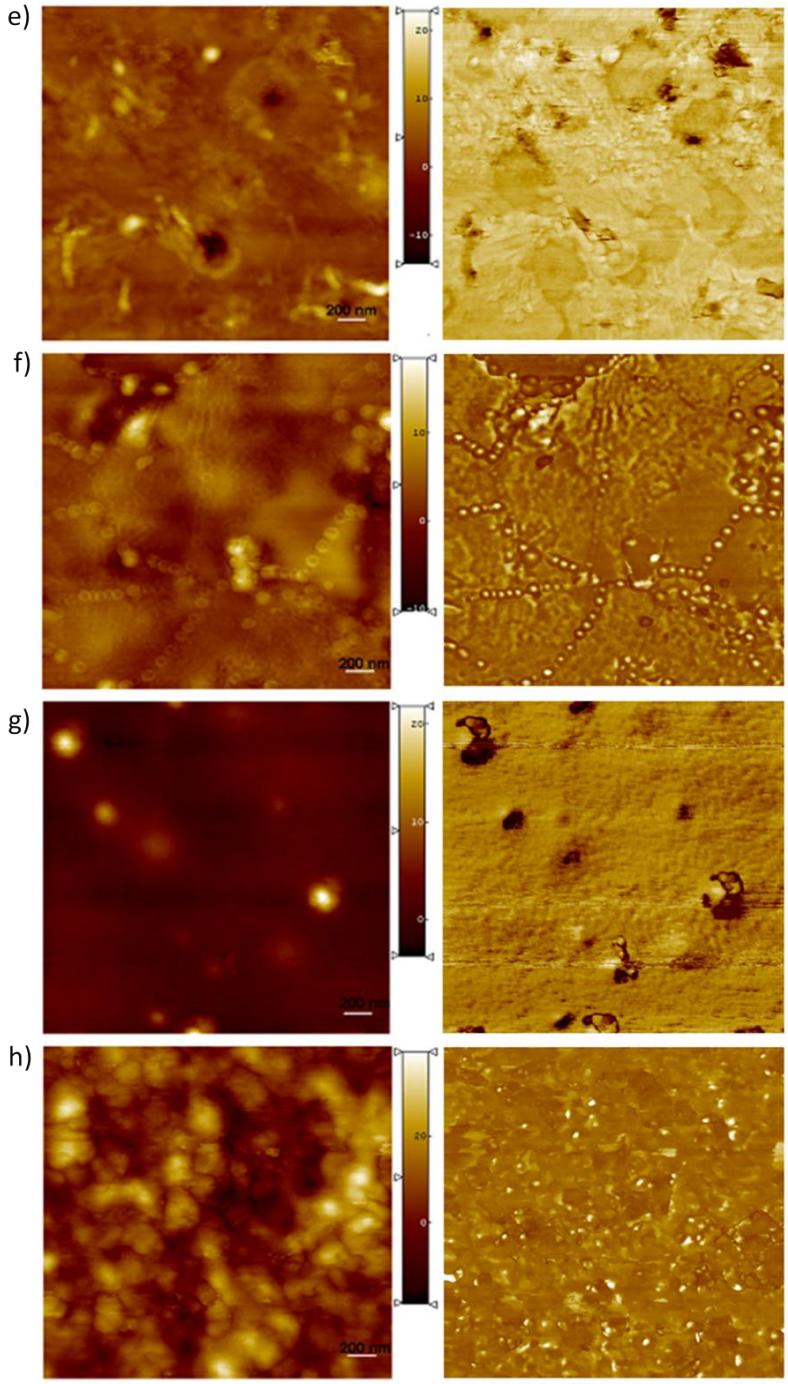


**Figure 17.** Representative AFM topographical and phase images of a) base paper, b) base paper with water treatment, c) base paper with MTEOS, d) base paper with OTEOS, e) impregnated paper, f) impregnated paper with water treatment, g) impregnated paper

with MTEOS, and h) impregnated paper with OTEOS. The image size is 2.5 µm x 2.5 µm. The scale bar is 200 nm.

The effect of different treatments on surface roughness of base and impregnated paper at macro-scale and micro-scale was investigated by CLSM and AFM and the results are compiled in Tables 5 and 6. As can be seen from Table 5, all the treatments decrease the surface roughness of base paper. However, the sol-gel coatings cause the largest decrease in RMS roughness in particular at the micro-scale. It is evident that MTEOS results in a smoother surface than OTEOS at both macro-scale and micro-scale. Furthermore, though no clear change in surface topography by water and heat treatment was observed from microscopic images, the treatment (the curing process) actually decreases the surface roughness. With respect to impregnated paper, water treatment increases the surface roughness at both macro- and micro-scale due to the exposed fibers (Figure 16b) which make the surface rougher after the treatment. MTEOS and OTEOS have different effects on the surface roughness at different length scales. At macro-scale, similar to the water treatment, MTEOS results in a slightly higher roughness compared to that of the untreated impregnated paper. The topographical features and roughness of MTEOS coating derive partially from the defects of the underlying impregnated paper; however, additional cracking and defects are very likely caused by the coating procedure and the coating itself (Figure 16c). The opposite result is found at micro-scale, i.e. a slightly lower roughness/smoother surface is obtained. OTEOS tends to result in a decreased surface roughness at macro-scale but an increased roughness due to the presence of granular structures at micro-scale (Figure 17h). OTEOS with the longer alkyl chains are hence concluded to increase the fine structure at micro scale but fill the cavities at macro scale more effectively than MTEOS.

**Table 5.** Surface roughness of paper samples measured by CLSM. The image size is 1.5 mm × 1.5 mm.

| *Samples* | *RMS roughness (µm)* |
|---|---|
| Bas paper | 27.2 |
| Base paper + water treatment | 18.5 |
| Base paper + MTEOS | 19.0 |
| Base paper + OTEOS | 21.5 |
| Impregnated paper | 23.3 |
| Impregnated paper + water treatment | 33.1 |
| Impregnated paper + MTEOS | 31.3 |
| Impregnated paper + OTEOS | 15.8 |

**Table 6.** Surface roughness of paper samples measured by AFM. The image size is 6 µm x 6 µm for base paper and 2.5 µm x 2.5 µm for PF impregnated paper.

| *Samples* | *RMS roughness (nm)* |
|---|---|
| Bas paper | 143.0 |
| Base paper + water treatment | 99.2 |
| Base paper + MTEOS | 26.0 |
| Base paper + OTEOS | 52.3 |
| Impregnated paper | 3.4 |
| Impregnated paper + water treatment | 3.7 |
| Impregnated paper + MTEOS | 2.5 |
| Impregnated paper + OTEOS | 8.0 |

***Surface chemistry***

XPS and ATR-FTIR were used to find out the effect of different treatments on the surface chemical properties of base paper and impregnated paper. The same treatments for the base paper and the industrial PF impregnated paper were used.

The average results from the XPS survey spectra measured from three different spots and their standard deviations are shown in Table 7. A higher atomic percent concentration of silicon is detected from the surface of the base paper with MTEOS than with OTEOS. This is logical result keeping in mind the longer aliphatic chain in OTEOS, which contributes to a stronger signal to carbon. It is also worth noting that the water treatment of base paper slightly decreases the surface carbon concentration and increases the oxygen concentration. This is probably due to the partial dissolution and migration of water soluble species, such as carboxylates, into the bulk during drying. For impregnated paper, after water treatment, a higher O/C ratio is found. This might be caused by previously partially cured PF resin which is further polycondensed/hardened during water and heat treatment. Similarly as for base paper, higher O/C and Si/C ratios are obtained for the paper with MTEOS than that with OTEOS. Furthermore, the atomic concentration of Na originating from the PF resin is lower for the sol-gel coated papers. A higher concentration of Na is found on the impregnated paper modified by water treatment. This is probably due to migration of Na onto the surface during the treatment.

The deconvolution and curve fitting results from the C1s XPS high resolution spectra are presented in Table 8. In general, the C1 represents the nonoxidized carbon, while C2–C3 refers to the oxidized carbon. The water and heat treatment resulted in a slight decrease of C1 compared to the untreated base paper. The decrease of C1 is quite similar to that observed as a result of an extraction process (Fardim 2005a). Only two peaks (C1–C2)

are resolved for both sol-gel coated samples. The C1 (C–C, C–H) peak was mainly attributed to the alkyl group in the coatings, while the C2 peak is ascribed to the C–O–Si or C–O–H bonds. In contrast to the reference and water-treated samples, the percentage of C2 is much less than that of C1 for both coatings. A marked difference is also found between the coatings; the C1/C2 ratio for MTEOS coating is ~5.6:1 whereas for OTEOS it is ~11.4:1. This difference reflects the difference between the length of the alkyl groups of MTEOS and OTEOS. The C3 and C4 components, which are characteristic of the fibers in the base paper, are not observed for sol-gel coated samples suggesting a rather complete coverage of the fibers on the paper surfaces by the applied coatings.

As for impregnated paper, the water treatment results in a decrease of C1 and C2 and a clear increase of C3. The increased concentration of the C3 component is likely due to the curing of the PF resin during the heating process, i.e. oligomers are formed through dimethylene ether linkages which may split to form aromatic aldehydes (Knop 1979). The C1/C2 ratio for MTEOS coating is ~7.5:1, whereas for OTEOS it is ~17.5:1.

It can also be seen from Table 7 and 8 that the highest O/C and Si/C is found for base paper with MTEOS. When compared to the base paper, with the same coating, lower ratios are observed on the surface of impregnated paper.

The ATR-FTIR results (Fig. 4, Paper IV) reveal that the water and heat treatment induces further curing of the PF resin, and the sol-gel coatings form the Si–O–C bonds with the hydroxyl groups in impregnated paper.

The distribution of sol-gel coatings on the paper surfaces were evaluated by ToF-SIMS imaging. The representative ToF-SIMS Si ion images are shown in Figures 18 & 19, which also contains the total positive ion images. High contrast (light) pixels in the images indicate high secondary ion peak intensities. Part of the differences in the intensities was caused by the topographical effects. The surface topography can be envisaged from the total ion images. In the Si ion images the intensity scale is set to the same level to compare the samples. Both the sol-gel coatings spread quite uniformly over the base paper and PF impregnated paper surfaces. Thin coating layers are presumably formed on base paper surfaces because the original texture of fibers is still visible. It is noted by SEM-EDS (Appendix II) that MTEOS is observed on both sides of base paper. This is probably due to the short aliphatic chain in MTEOS, which allows it penetrate easier.

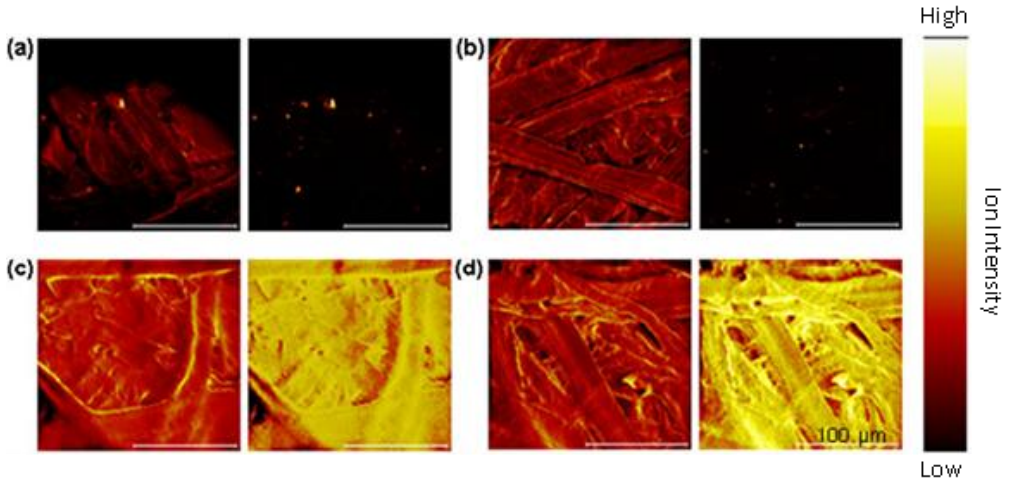


**Figure 18.** Positive total ion (left) and $Si^{4+}$ ion (right) ToF-SIMS images of (a) base paper, (b) base paper with water treatment, (c) base paper with MTEOS, and (d) base paper with OTEOS. The scale bar is 100 µm.

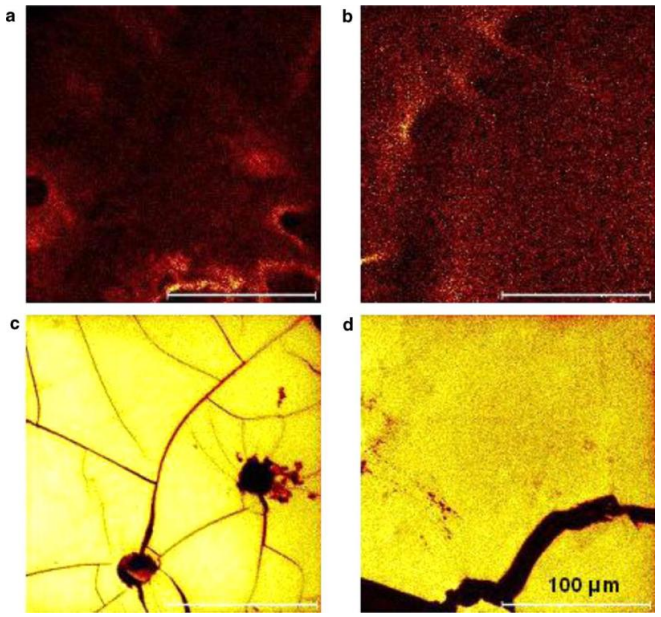


**Figure 19.** ToF-SIMS Si ion distribution on the surfaces of (a) impregnated paper, (b) impregnated paper with water treatment, (c) impregnated paper with MTEOS, and (d) impregnated paper with OTEOS. The scale bar is 100 µm.

**Table 7.** Surface atomic compositions (%) of the studied paper samples. The standard deviations from three measured spots are in parentheses.

| *Samples* | *C %* | *O %* | *Na %* | *Si %* | *O/C* | *Si/C* |
|---|---|---|---|---|---|---|
| Base paper | 64.8 (1.3) | 34.5 (1.1) | − | 0.7 (0.4) | 0.53 | 0.011 |
| Base paper + water treatment | 62.4 (1.4) | 37.6 (1.4) | − | <0.1 | 0.60 | − |
| Base paper + MTEOS | 17.3 (0.4) | 59.7 (1.0) | − | 23.0 (0.9) | 3.45 | 1.33 |
| Base paper + OTEOS | 39.9 (0.8) | 44.1 (0.8) | − | 16.0 (0.6) | 1.10 | 0.40 |
| PF impregnated paper | 87.0 (3.0) | 10.1 (1.9) | 2.7 (1.4) | 0.2 (0.3) | 0.12 | 0.002 |
| PF impregnated paper + water treatment | 72.0 (1.4) | 17.6 (0.7) | 10.3 (0.8) | <0.1 | 0.24 | − |
| PF impregnated paper + MTEOS | 28.3 (2.5) | 51.6 (2.3) | 0.2 (0.4) | 19.9 (0.2) | 1.82 | 0.70 |
| PF impregnated paper + OTEOS | 44.5 (1.3) | 40.5 (1.0) | <0.1 | 15.0 (0.4) | 0.91 | 0.34 |

**Table 8.** XPS C1s peak deconvolution results for the studied paper samples. The standard deviations from three measured spots are in parentheses.

| *Samples* | *C1 (C–C, C–H)* | *C2 (C–O–C, C–OH)* | *C3 (O–C–O, C=O)* | *C4 (O–C=O)* |
|---|---|---|---|---|
| Base paper | 38.0 (5.9) | 49.5 (6.1) | 10.2 (2.4) | 2.3 (2.1) |
| Binding energy (eV) | 284.8 | 286.4 | 287.8 | 288.9 |
| Base paper + water treatment | 31.6 (1.5) | 53.2 (2.3) | 13.3 (0.5) | 2.0 (0.3) |
| Binding energy (eV) | 284.8 | 286.4 | 287.8 | 288.9 |
| Base paper + MTEOS | 84.8 (1.2) | 15.2 (1.2) | – | – |
| Binding energy (eV) | 284.8 | 286.7 | | |
| Base paper + OTEOS | 91.7 (1.1) | 8.3 (1.1) | – | – |
| Binding energy (eV) | 284.8 | 286.7 | | |
| PF impregnated paper | 95.6 (0.9) | 4.4 (0.9) | – | – |
| Binding energy (eV) | 284.8 | 286.3 | | |
| PF impregnated paper + water treatment | 89.1 (0.8) | 3.7 (0.6) | 7.2 (0.9) | – |
| Binding energy (eV) | 284.8 | 286.3 | 288.2 | |
| PF impregnated paper + MTEOS | 88.2 (2.5) | 11.8 (1.3) | – | – |
| Binding energy (eV) | 284.8 | 286.3 | | |
| PF impregnated paper + OTEOS | 94.6 (0.8) | 5.4 (0.8) | – | – |
| Binding energy (eV) | 284.8 | 286.3 | | |

***Water repellency***

The sol-gel coatings (MTEOS) and OTEOS) were used in order to modify the surface energy. The two coatings containing either a short ($–CH_3$) or a longer organic aliphatic chain ($–CH_3(CH_2)_7$), led to differences in the hydrophobicity of paper substrates. The water contact angle results (Figure 20) show that both coatings reduce the hydrophilicity of base paper and PF impregnated paper resulting in an approximate water contact angle of ~80° and ~105°, respectively. The water contact angle of the untreated and water-treated paper was hardly measurable, because a water droplet placed on the paper surface penetrated completely into the paper after only a few seconds. The droplet volumes were

also recorded for evaluation of penetration of water through the paper surfaces. As a non-permeable reference surface, a polypropylene film was used. The decrease in volume of the droplets on the polypropylene (PP) surface is due to evaporation of water, i.e. no penetration of water through the plastic film takes place. The wetting ability and absorptivity of base paper is clearly reduced by both sol-gel coatings. Only evaporation and slight spreading of water droplets took place on the sol-gel coated surfaces within 600 s. The volumes of the water droplets on the samples treated with MTEOS and OTEOS are found to decline at the same slow kinetics as that measured on a completely non-permeable polypropylene film. This indicates that only evaporation of water takes place on those surfaces. Consequently, the absorptivity of base paper is clearly reduced by both sol-gel coatings as the surface is mostly covered by silica coatings and cellulose is not easily accessible to water. These results indicate that the alkyl chain length in alkoxysilane has an impact on the hydrophobicity of the coated base paper. This coincides well with earlier studies where a longer alkyl chain has been found to result in a higher hydrophobicity (Zhu 2011, Textor 2010). It can be concluded that in our case, MTEOS with only one carbon in its alkyl group is not effective enough to impart adequate hydrophobicity to the base paper though it reduces the absorptivity. The higher hydrophobicity of OTEOS is also partly attributed to its higher surface roughness as revealed by AFM (Table 6).

The water contact angle for the untreated impregnated paper is 20°, indicating a relatively hydrophilic surface. Furthermore, a sudden drop in the contact angle is observed after ca. 2 minutes indicating absorption. When the paper sample was sprayed with water and heat-treated, the contact angle is increased to ~80°. This is due to the partial curing of the PF on the paper surface. MTEOS yields a slightly more hydrophilic surface than water treatment, the contact angle being ~70°. OTEOS yields a hydrophobic surface with a contact angle of ~105°. The more hydrophobic nature of the OTEOS compared to the MTEOS is due to the longer aliphatic chains. The changes in droplet volumes on the MTEOS and OTEOS surfaces are equal with the ones on the PP surface, which indicates that only evaporation is reducing the droplet volume. The calculated surface energies, divided into polar and dispersive components, for impregnated paper after different treatments (Fig. 8, Paper IV) indicate that OTEOS leads to a less polar surface than MTEOS, which in turn is more polar than the reference (the impregnated paper with water and heat treatment). This is very likely due to the long aliphatic (non-polar) chains of OTEOS. The difference between the dispersive component of the surface energy of MTEOS and OTEOS surfaces is not significant.

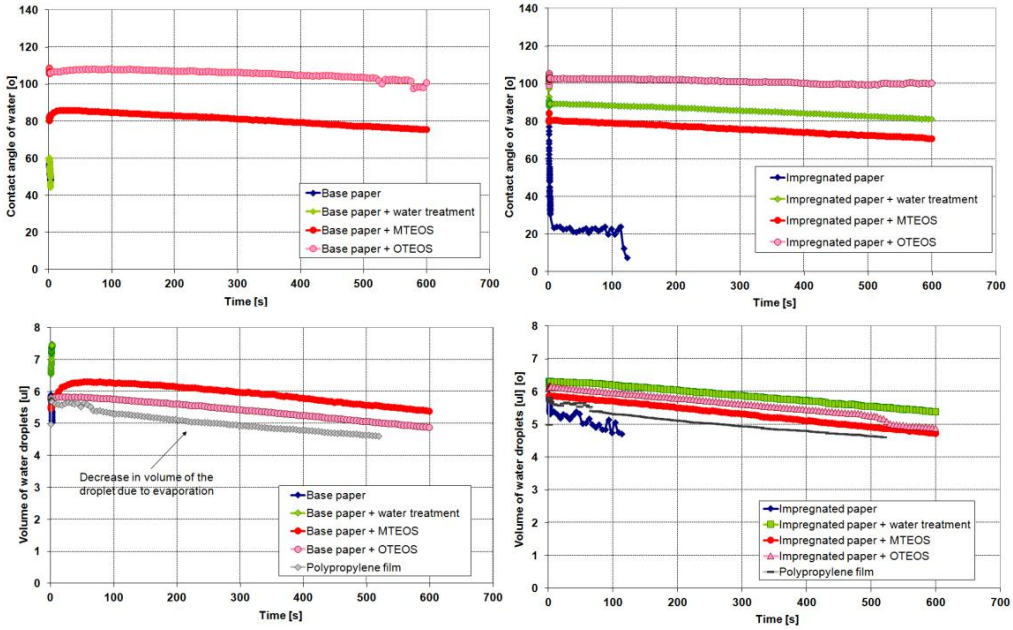


**Figure 20.** The water contact angle measurements for reference and treated base paper and PF impregnated paper. The polypropylene film was used as a non-penetrating reference surface.

### 5.4 Surface characteristics of laminated plywood

In this section, the surface chemical properties and water absorption of the laminated plywood surfaces is discussed. The description of the analyzed laminated plywood samples are comprised in Table 9. The sol-gel coatings for paper to be pressed onto plywood are OTEOS which contains an octyl group and FTEOS which contains a fluorocarbon group. The description of the paper samples including the treatments is presented in Table 3. Surface properties of these papers before lamination will be also discussed.

**Table 9.** Plywood samples.

| *Samples* | *Treatment* | *Treatment conditions* |
|---|---|---|
| Ply 1 | Base paper pre-coated with OTEOS before impregnation with PF (coating amount 1.3 g/m$^2$, dry weight) | After OTEOS coating, paper was dried in an oven at 110ºC for 15 minutes before impregnation with PF, after impregnation pre-curing in an oven at 160ºC for 20-25 seconds before pressing on top of plywood |
| Ply 2 | Base paper pre-coated with FTEOS before impregnation with PF (coating amount 0.8 g/m$^2$, dry weight) | After FTEOS coating, paper was dried in an oven at 110ºC for 15 minutes before impregnation with PF, after impregnation pre-curing in an oven at 160ºC for 20-25 seconds before pressing on plywood |
| Ply 3 | Industrially impregnated paper treated with OTEOS (coating amount 0.6 g/m$^2$, dry weight) | After coating, paper was dried in the oven at 110°C for 15 min, then pressed on top of plywood |
| Ply 4 | Industrially impregnated paper treated with FTEOS (coating amount 1.1 g/m$^2$, dry weight) | After coating, paper was dried in an oven at 110°C for 15 min, then pressed on top of plywood |
| Ply 5 | Base paper impregnated with a mixture of OTEOS and PF, the amount of OTEOS coating was 0.5% of the dry weight of the PF-resin | After impregnation, paper was pre-cured in an oven at 160ºC for 20-25 seconds before pressing on top of plywood |
| Ply 6 | Base paper impregnated with a mixture of FTEOS and PF, the amount of FTEOS coating was 0.5% of the dry weight of the PF-resin | After impregnation, paper was pre-curing in an oven at 160ºC for 20-25 seconds before pressing on top of plywood |
| Reference 1 | Industrially impregnated paper | Pressing on top of plywood |

| | | |
|---|---|---|
| Reference 2 | Manually impregnated paper | After manual impregnation, paper was pre-cured in an oven at 160ºC for 20-25 seconds before pressing on plywood |

Figure 21 shows AFM phase images of the base paper and the industrially impregnated paper before and after the sol-gel coatings. The AFM images were captured at the fiber surfaces for the base paper samples and defect-free areas for the impregnated paper samples. OTEOS appears to produce a better micro-scale coverage of the fiber surfaces than FTEOS. For the impregnated paper, application of different coatings results in different micro-structures. Films and patches are observed on the surface of impregnated paper with OTEOS. On the other hand, the surface of the impregnated paper lacks the particulate microstructure seen after the application of FTEOS.

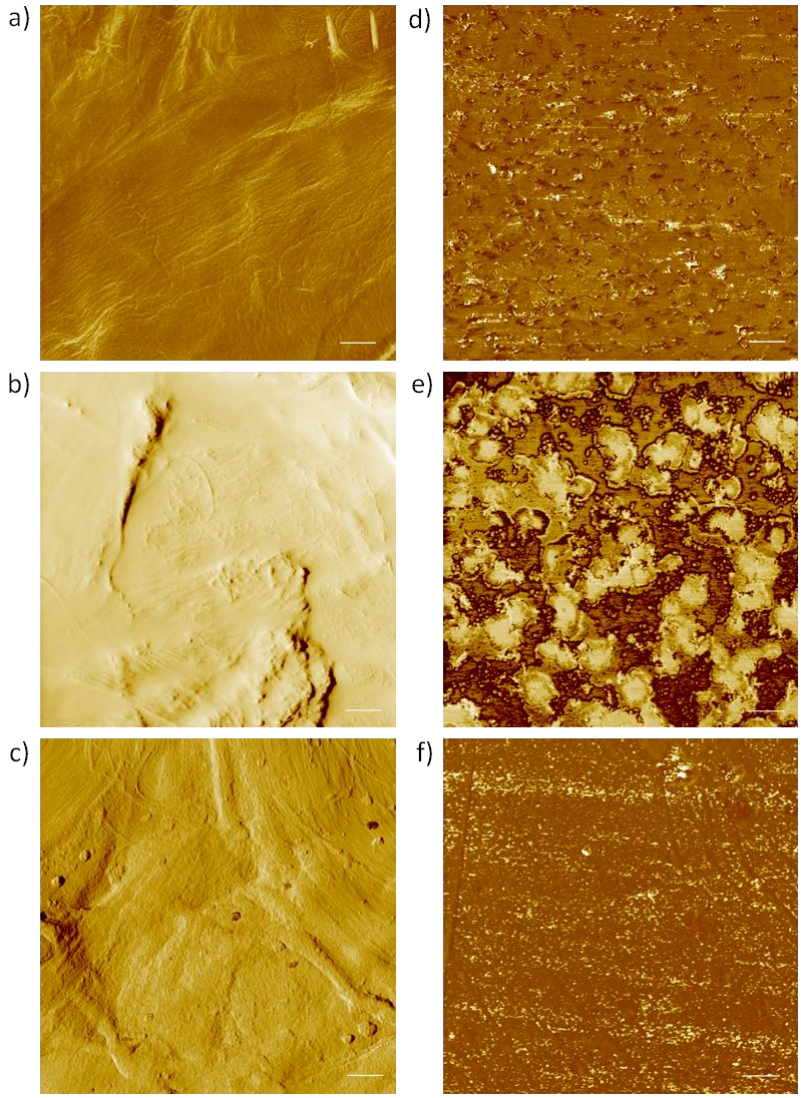


**Figure 21.** Representative AFM phase images of (a) base paper, (b) with OTEOS, (c) with FTEOS, (d) industrially impregnated paper, (e) with OTEOS and (f) with FTEOS. The image size is 10 µm x 10 µm. The scale bar is 1 µm.

The surface roughness of uncoated and coated base paper and industrially impregnated paper measured by AFM is summarized in Table 10. The roughness values indicate that base paper has a much higher small-scale surface roughness (at correlation length T < 2 µm) compared to the impregnated paper. Both coatings have a smoothening effect on the fiber surfaces of base paper by mostly covering the microfibril bundles as shown in Figures 21b and 21c. On the other hand, OTEOS slightly increases, while FTEOS decreases the surface roughness of the industrially impregnated paper at the measured

short length scale (T < 1 µm). This is in good agreement with the previous findings that at micro-scale OTEOS decreased the surface roughness of base paper while increase the surface roughness of industrially impregnated paper (findings in section 5.3). The macro-roughness (Table 11) of the base paper samples calculated based on the CLSM images reveals that both coatings filled the voids between adjacent fibers.

**Table 10.** Surface roughness of paper samples by AFM. The standard deviations from 6 topographical images are in parentheses. The image size is 10 µm × 10 µm.

| *Samples* | *$S_q$ ± STD (nm)* | *Correlation length, T (nm)* |
|---|---|---|
| Base paper | 252 ± 45 | 1656 |
| Base paper + OTEOS | 145 ± 31 | 1245 |
| Base paper + FTEOS | 115 ± 20 | 1483 |
| Industrially impregnated paper | 17.9 ±4.6 | 418 |
| Industrially impregnated paper + OTEOS | 22.1 ± 7.2 | 697 |
| Industrially impregnated paper + FTEOS | 9.7 ± 2.8 | 584 |

**Table 11.** Surface roughness for base paper samples by CLSM. The image size is 1.5 mm × 1.5 mm.

| *Parameters* | *Units* | *Base paper* | *Base paper + OTEOS* | *Base paper + FTEOS* |
|---|---|---|---|---|
| $S_q$ | µm | 5.7 | 4.9 | 5.0 |
| Correlation length, T | µm | 46.9 | 98.5 | 64.5 |

The surface chemistry of the uncoated and coated papers was studied by XPS. The results from survey spectra are listed in Table 12. The highest Si, O/C and Si/C are observed from base paper with coating B. The elemental composition of impregnated paper is not changed significantly by either coating. The results from the high resolution spectra (Table 13) show that both coatings increase the percentage of non-oxidized carbon (C1) for the base paper. However, this is not seen for impregnated paper as no obvious changes in the C1-C2 can be seen after the coatings.

**Table 12.** Surface elemental compositions (atomic %) of paper samples by XPS. The results are averages from three measured spots and the standard deviations are in parentheses.

| *Paper samples* | *C* | *O* | *Si* | *Na* | *F* | *O/C* | *Si/C* |
|---|---|---|---|---|---|---|---|
| Base paper | 64.8 (1.3) | 34.5 (1.1) | 0.7 (0.4) | <0.1 | <0.1 | 0.53 | 0.01 |
| Base paper + OTEOS | 43.3 (0.8) | 40.8 (0.5) | 15.9 (0.5) | <0.1 | <0.1 | 0.94 | 0.37 |
| Base paper + FTEOS | 59.6 (1.3) | 37.1 (0.4) | 2.5 (1.0) | 0.4 (0.3) | 0.5 (0.3) | 0.62 | 0.04 |
| Industrially impregnated paper | 92.1 (1.6) | 7.4 (1.3) | 0.3 (0.2) | 0.1 (0.1) | <0.1 | 0.08 | 0.00 3 |
| Industrially impregnated paper + OTEOS | 91.8 (0.8) | 7.1 (0.8) | 0.9 (0.4) | 0.2 (0.5) | <0.1 | 0.08 | 0.01 |
| Industrially impregnated paper + FTEOS | 92.6 (1.7) | 6.4 (1.4) | 0.2 (0.3) | 0.6 (0.2) | 0.2 (0.3) | 0.07 | 0.00 2 |

**Table 13.** XPS results from the resolved C1s peaks of paper samples. The standard deviations from three measured spots are in parentheses.

| *Paper samples* | *C1% (C–C, C–H)* | *C2% (C–OH, C–O–C)* | *C3% (O–C–O, C=O)* | *C4% (O–C=O)* |
|---|---|---|---|---|
| Base paper | 38.0 (5.9) | 49.5 (6.1) | 10.2 (2.4) | 2.3 (2.1) |
| Base paper + OTEOS | 84.9 (2.4) | 12.6 (2.0) | 2.5 (0.6) | – |
| Base paper + FTEOS | 41.1 (1.5) | 46.0 (2.8) | 11.8 (1.8) | 1.1 (0.4) |
| Industrially impregnated paper | 95.6 (0.9) | 4.4 (0.9) | – | – |
| Industrially impregnated paper + OTEOS | 95.4 (1.0) | 4.6 (1.0) | – | – |
| Industrially impregnated paper + FTEOS | 96.5 (0.5) | 3.5 (0.5) | – | – |

The distributions of sol-gel coatings on the base paper and the industrially impregnated paper were analyzed by mapping of Si with ToF-SIMS positive mode. Representative ToF-SIMS total positive ion, Si and Na images are shown in Figure 22. OTEOS spreads more uniformly on the surface of base paper than FTEOS. This agrees with the AFM

results that OTEOS likely has a more complete coverage than FTEOS. The distribution of sol-gel coatings on the surface of impregnated paper is difficult to interpret due to the low intensity of Si ion detected by ToF-SIMS. However, according to the SEM-EDS images (Appendix III), the coatings are discontinuously formed on the impregnated paper.

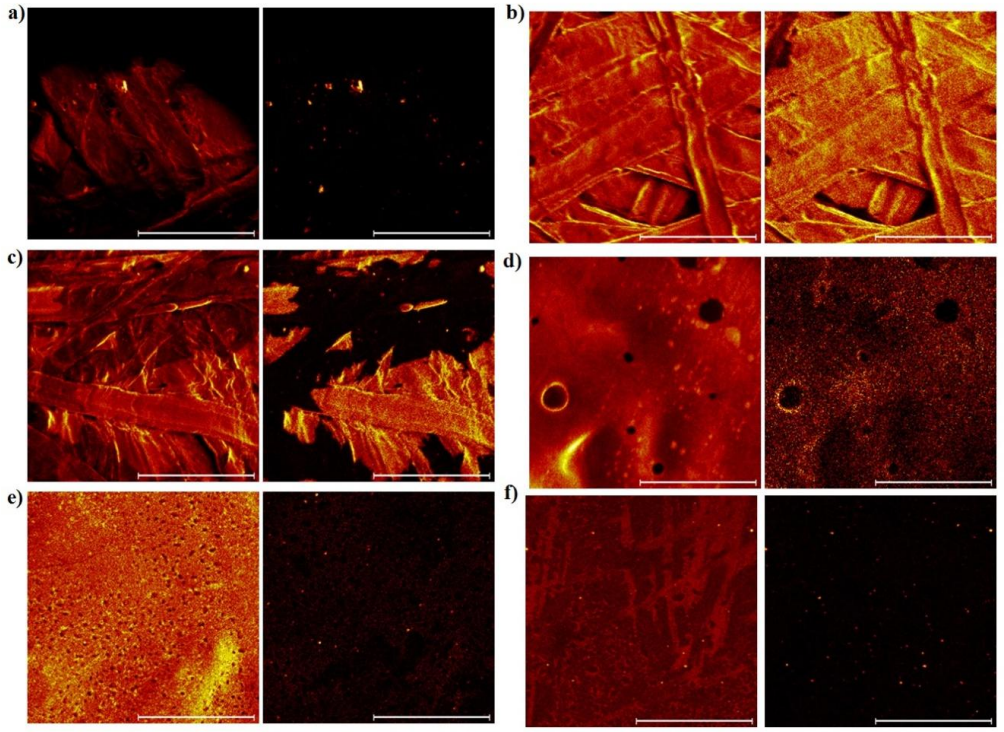


**Figure 22.** ToF-SIMS total positive ion (left) and $Si^{4+}$ (right) imaging of (a) base paper, (b) with OTEOS, (c) with FTEOS, (d) industrially impregnated paper, (e) with OTEOS and (f) with FTEOS. The scale bar is 100 μm.

The surface chemistry and water absorption of the laminated plywood was studied by XPS, ToF-SIMS and Cobb test. The XPS results are shown in Table 14. Higher O/C and Si/C ratios are apparent on the surface of Ply 3.

**Table 14.** Surface elemental compositions (atomic %) of plywood samples by XPS. The standard deviations from three measured spots are in parentheses.

| *Plywood samples* | *C* | *O* | *Si* | *Na* | *F* | *O/C* | *Si/C* |
|---|---|---|---|---|---|---|---|
| Ply 1 | 81.8 (1.4) | 14.4 (1.3) | 0.7 (0.7) | 3.4 (0.8) | <0.1 | 0.18 | 0.008 |
| Ply 2 | 79.6 (0.5) | 15.8 (0.5) | 0.7 (0.3) | 2.9 (0.7) | 1.0 (0.2) | 0.20 | 0.009 |
| Ply 3 | 69.3 (1.2) | 22.5 (0.6) | 5.2 (0.2) | 3.1 (0.6) | <0.1 | 0.32 | 0.08 |
| Ply 4 | 75.6 (1.3) | 17.1 (1.1) | 2.3 (0.4) | 3.0 (0.6) | 2.0 (0.5) | 0.23 | 0.03 |
| Ply 5 | 84.3 (1.3) | 12.5 (1.2) | 0.4 (0.3) | 2.8 (0.5) | <0.1 | 0.15 | 0.005 |
| Ply 6 | 80.6 (0.8) | 15.8 (0.7) | 0.9 (0.3) | 2.5 (0.4) | 0.2 (0.3) | 0.20 | 0.01 |
| Reference 1 | 75.0 (1.6) | 18.5 (0.4) | 1.1 (0.3) | 5.3 (0.9) | <0.1 | 0.25 | 0.01 |
| Reference 2 | 80.3 (1.5) | 15.0 (0.7) | 1.4 (0.1) | 3.3 (1.0) | <0.1 | 0.19 | 0.02 |

Regarding the plywood pressed with manually impregnated paper, the comparison was made between the reference plywood (Reference 2, Table 9) and the relevant laminated plywood (Ply 1, Ply 2, Ply 5, Ply 6, Table 9). The slightly lower O/C and Si/C ratios are seen for Ply 1 and Ply 5 compared to Reference 2 and Ply 2 and Ply 6. Relatively high amounts of Si and Na on the reference plywood surfaces are likely from the release paper used during the pressing.

The chemical bonds present on the surfaces of the laminated plywood from XPS C1s high resolution spectra are shown in Table 15. Three peaks (C1–C3) are resolved from all the laminated plywood samples. In general, no prominent differences in the chemical bonds between the samples can be detected. The content of C1 (C–C, C–H) is slightly increased for Ply 3 and Ply 4 in comparison to the reference 1. No significant difference exists between Ply 1, Ply 5 and the reference 2. Very slight decrease in C1 and increase in C2 component is evident for Ply 2, Ply 6 compared to the Reference 2. In addition, one can note that the third peak C3 (O–C–O, C=O) is observed on the surface of the industrially impregnated paper (Reference 1, Table 15). The pressing probably has a similar effect as water and heat treatment to the industrially impregnated paper as stated previously (Table 8). The C3 might also derive from contaminates during the pressing.

**Table 15.** XPS results from resolved C1s peaks of plywood samples. The standard deviations from three measured spots are in parentheses.

| *Plywood samples* | *C1% (C–C, C–H)* | *C2% (C–O, C–O–C)* | *C3% (O–C–O, C=O)* | *C4% (O–C=O)* |
|---|---|---|---|---|
| Ply 1 | 94.3 (0.6) | 1.6 (0.3) | 4.1 (0.3) | – |
| Ply 2 | 92.8 (0.8) | 3.0 (0.1) | 4.2 (0.7) | – |
| Ply 3 | 92.6 (0.7) | 2.9 (0.1) | 4.5 (0.7) | – |
| Ply 4 | 92.8 (0.4) | 2.8 (0.5) | 4.4 (0.4) | – |
| Ply 5 | 94.3 (1.0) | 1.9 (0.4) | 3.8 (0.6) | – |
| Ply 6 | 92.8 (0.9) | 3.0 (0.7) | 4.2 (0.5) | – |
| Reference 1 | 91.6 (0.6) | 2.9 (0.7) | 5.5 (1.0) | – |
| Reference 2 | 94.2 (0.4) | 1.6 (0.3) | 4.2 (0.5) | – |

The distribution of the sol-gel coatings on the film-coated plywood samples was evaluated by ToF-SIMS imaging (Figure 23). It appears that all the coatings spread unevenly on the plywood surfaces.

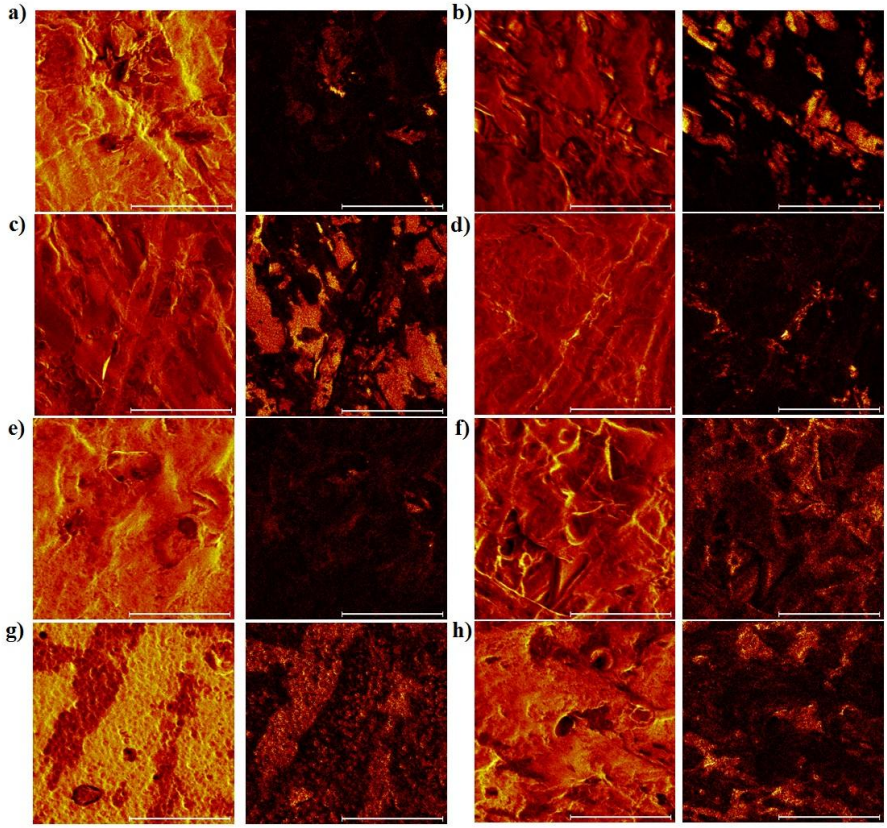


**Figure 23.** ToF-SIMS total positive ion (left) and $Si^{4+}$ (right) imaging of laminated plywood (a) Ply 1, (b) Ply 2, (c) Ply 3, (d) Ply 4, (e) Ply 5, (f) Ply 6, (g) Reference 1 and (h) Reference 2. The scale bar is 100 µm.

The effect of the impregnated paper on the water absorption of the laminated plywood is shown in Figure 24. When the impregnations are carried out in the laboratory, considerable variation in the water absorption values is seen (Figure 24b). Due to the variations it is difficult to assess the real effect of the sol-gels on the water absorption properties. However, it can be seen that pre-coating of the base paper with the sol-gels before impregnation (Ply 1, Ply 2) does not decrease water absorption. By coating the industrially impregnated paper with OTEOS (Ply 3), a slight decrease in the water absorption values can be seen (Figure 24a). In addition, impregnation of the base paper with the mixture of OTEOS coating and PF-resin (Ply 5) shows a clear decrease in the water absorption values compared to the reference (Reference 2). The FTEOS coating (Ply 4, Ply 6) seemed to have a smaller influence on the water absorption values than OTEOS. This is probably due to the short chain ($CF_3$–) FTEOS has, which has a less steric effect for the paper/plywood from interaction with water.

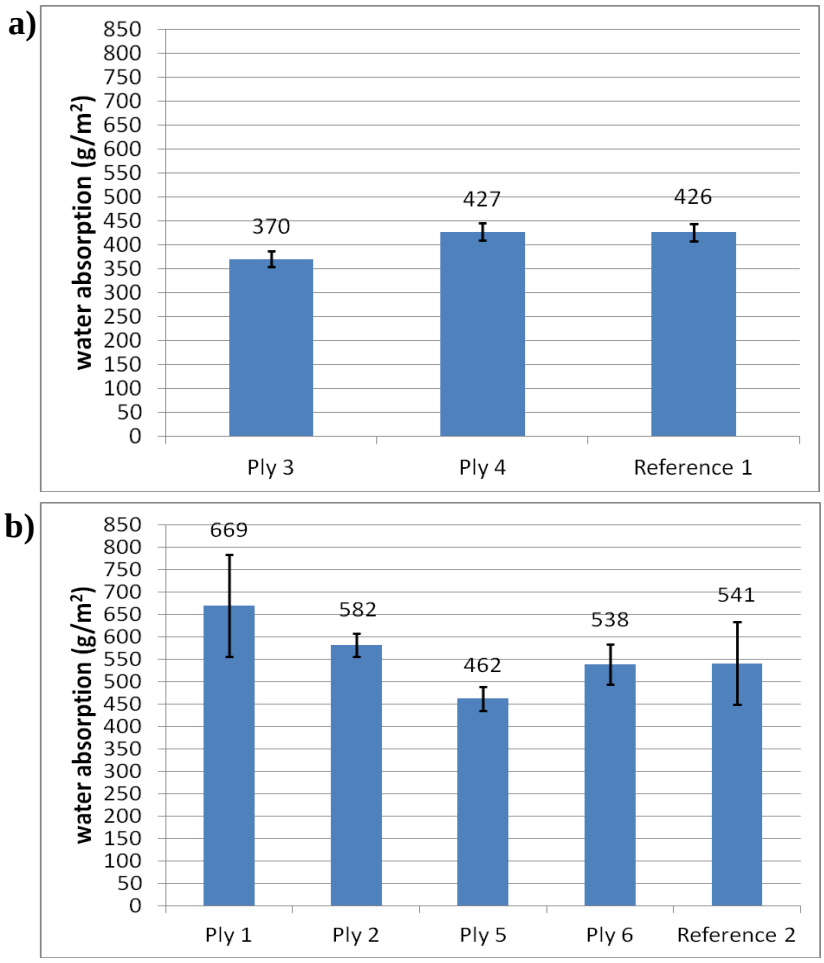


**Figure 24.** Water absorption of film-coated plywood samples after seven days. The error bars are the standard deviations from 3–10 measurements.

# 6. CONCLUSIONS

Light microscopy, AFM and FE-SEM are suitable tools to characterize fiber wall surface structures. Single fiber examination with a combination of these techniques provides an insight into the fiber wall surface structure. Distinction between the outer (ML/P) and the exposed inner ($S_2$) fiber walls in TMP refined fibers can easily be done by light microscopy in transmitted light on fibers stained with Rhodamine Red. Both high resolution FE-SEM and AFM give qualitative information in form of visual characterization of fiber surface structures. The strength of AFM lies in additional possibilities to quantify surface roughness and other surface structural characteristics.

Using AFM, the surface structures of the inner ($S_2$) and outer (ML/P) fiber wall areas are clearly distinguishable based on their fibril angle and RMS roughness values. The remnants of the outer fiber areas in all the studied samples are found rougher than the exposed inner fiber wall areas. The buffered sodium oxalate treatment increases mostly the outer fiber wall roughness. The hydrochloric acid treatment is suggested to create surface pores on the inner ($S_2$) fiber wall areas by hydrolyzing and removing some hemicelluloses from the $S_2$ fiber walls. The hydrochloric acid treatment also reveals the appearance of a granular structure, probably lignin, on the $S_2$ fiber walls.

A successful deposition of sol-gel coatings (octyltriethoxysilane and methyltriethoxysilane) on the studied wood surfaces is observed. The deposited sol–gel coatings appeared as particulate- and/or film- like structures. MTEOS had a stronger tendency than OTEOS to smoothen the wood surfaces at the studied micro-scale. The coatings are found to spread fully on the pine sapwood surfaces, especially into cell walls. Thin coating layers are formed on the heat-treated spruce surfaces following the wood original surface structure. These results are in good agreement with the contact angle results showing that the moisture tolerance of the coated surfaces, especially the ones coated with the more hydrophobic sol-gel (octyltriethoxysilane), is enhanced compared to the non-coated references. With the same coating amount, less coating is covalently bound to the heat-treated spruce surface than pine sapwood.

The surface and wetting properties of base paper are clearly changed by the applied sol-gel coatings. Discontinuous thin films are formed on base paper surfaces. The fiber surfaces are covered by the sol-gel coating, but the fiber-fiber intersections were only partially filled. The sol-gel coatings, as well as the water treatment (curing process), decrease the surface roughness at both macro- and micro-scale. Octyltriethoxysilane resulted in a rougher surface than methyltriethoxysilane. Octyltriethoxysilane decreased more effectively the wettability of base paper. The results show that the surface energetics, i.e. the wetting and absorptive properties of paper samples, can be adjusted by

the sol-gel coatings. The coating method is easy and straightforward to use, and tailoring the properties of the sol-gel materials can be used to tune the thickness, homogeneity and degree of hydrophobicity of the formed coatings. Further studies are needed to optimize the coating conditions to control the coating of the intersections between the fibers.

With respect to the impregnated paper, water treatment increases its surface roughness and induces further curing of the PF resin. Methyltriethoxysilane results in a slightly smoother surface than water treatment. In general, octyltriethoxysilane decreases the surface roughness at macro-scale but increases the surface roughness at micro-scale due to the presence of granular structures on impregnated paper. Both coatings are evenly distributed on the paper surface forming Si–O–C bonds with the hydroxyl groups. In comparison with the reference treatment (water treatment), the sol-gel coatings increase the hydrophobicity of the impregnated paper with an impermeable surface. Fluorocarbon-containing triethoxysilane decreased the surface roughness of base paper and industrially PF impregnated paper at micro-scale. However, it was unevenly distributed on the paper surface. For plywood samples, the most effective decrease in water absorption is obtained by a mixture of the PF resin and octyltriethoxysilane coating.

In conclusion, the sol-gel coatings were found applicable for controlling surface properties of wood and wood-based products. The surface roughness of the modified wood or paper is scale-dependent. At micro-scale, MTEOS as well as FTEOS appear smoother than OTEOS, which is attributed to MTEOS/FTEOS being more inclined to form thin films due to its short chain length. At macro-scale, the surface roughness is determined by the sol-gel coating coverage as well as the substrate. Octyltriethoxysliane is found to provide a higher hydrophobicity than the two other coatings under consideration in this study.

By combining advanced surface analytical tools, it is possible to gain insight into the surface properties of sol-gel modified wood and paper. AFM and CLSM enable characterization of the surface morphology of the modified at micro and macro scales, while XPS and ToF-SIMS provide complementary information of the surface chemical composition and uniformity of the sol-gel coatings.

## REFERENCES


Abramowitz, M., Davidson, M. W. (2007). Introduction to Microscopy, Molecular Expressions. Retrieved October 28, 2013, from Molecular Expressions Microscopy Primer: Anatomy of the Microscope – Introduction: http://micro.magnet.fsu.edu/primer/anatomy/introduction.html

Adamson, A. W. (1967). *Physical chemistry of surfaces*. 2nd ed., Interscience, New York.

Adusumalli, R. –B., Raghavan, R., Schwaller, P., Zimmermann, T., Michler, J. (2010). In situ SEM micro-indentation of single wood pulp fibres in transverse direction. *Journal of Electron Microscopy (Tokyo)*, 59(5) 345-349.

Alén, R., Kotilainen, R., Zaman, A. (2002). Thermochemical behavior of Norway spruce (Picea abies) at 180-225 ºC. *Wood Science and Technology*, 36, 163–171.

Amerio, E., Sangermano, M., Malucelli, G., Priola, A., Voit, B. (2005). Preparation and characterization of hybrid nanocomposite coatings by photopolymerization and sol-gel process. *Polymer*, 46, 11241-11246.

Ayadi, N., Lejeune, F., Charrier, F., Charrier, B., Merlin, A. (2003). Color stability of heat-treated wood during artificial weathering, *Holz als Roh- und Werkstoff*, 61(3), 221-226.

Bardage, S., Donaldson, L., Tokoh, C., Daniel, G. (2004). Ultrastructure of the cell wall of unbeaten Norway spruce pulp fibre surfaces. *Nordic Pulp and Paper Research*, 19(4), 448-452.

Bente, M., Avramidis, G., Föster, S., Rohwer, E. G., Viöl, W. (2004). Wood surface modification in dielectric barrier discharges at atmospheric pressure for creating water repellent characteristics. *Holz als Roh-und Werkstoff*, 62, 157-163.

Bexell, U. (2003). *Surface Characterization Using ToF-SIMS, AES and XPS of Silane Films and Organic Coatings Deposited on Metal Substrates*. Doctoral thesis, Uppsala University, Uppsala, Sweden.

Bico, J., Thiele, U., Quéré, D. (2002). Wetting of Textured Surfaces. *Colloids and surfaces A: physicochemical and engineering aspects*, 206, 41-46.

Binnig, G., Rohrer, H. (1986). Scanning Tunneling Microscopy-From Birth to Adolescence. Physics, Nobel lecture, 389-409.

Boonstra, M. J., Rijsdijk, J. F., Sander, C., Kegel, E., Tjeerdsma, B., Militz, H., Van Acker, J., Stevens, M. (2006). Microstructural and physical aspects of heat treated wood. Part 2. Hardwoods. *Maderas. Ciencia y Tecnologia*, 8(3), 193–208.

Braaten, K. R. (1997). The impact of fiber geometry, fiber splitting and fibrillation on light scattering. *International Mechanical Pulping Conference (IMPC)*, Stockholm, Sweden.

Brandon, S., Haimovich, N., Yeger, E., Marmur, A. (2003). Partial wetting of chemically patterned surfaces: The effect of drop size. *Journal of Colloid and Interface Science*, 263, 237-243.

Brinen, J. S. (1993). The observation and distribution of organic additives on paper surfaces using surface spectroscopic techniques. *Nordic Pulp and Paper Research Journal*, 8, 123-129.

Brochier Salon, M. -C. Abdelmouleh, M. Boufi, S. (2005). Silane adsorption onto cellulose fibers: hydrolysis and condensation reactions. *Journal of Colloid and Interface Science*, 289, 249-261.

Bryne, L. E. (2008). *Aspects on wettability and surface composition of modified wood*. Licentiate thesis, KTH-Stockholm, Sweden.

Buchanan, J.G., Washburn, O.V. (1962). The surface and tensile fractures of chemical fibre hand sheets as observed with the Scanning electron microscope. Technical Report, Pulp and Paper Research Institute of Canada, No.294.

Börås, L., Gatenholm, P. (1999). Surface composition and morphology of CTMP fibers. *Holzforschung*, 53, 188-194.

Cassie, A. B. D., Baxter, S. (1944). Wettability of porous surfaces. *Transactions of the Faraday Society*, 40, 546-551.

Cassie, A. B. D. (1948). Contact angles. *Discussions of Faraday Society*, 3, 11-16.

Chang, C.I., Keith, C.T. (1978). Properties of heat-darkened wood. II. Mechanical properties and gluability. Report, Eastern Forest Products Laboratory, Canada, No. OPX214E.

Correia, N. T., Ramos, J. M. M., Saramago, B. J. V., Calado, J. C. G. (1997). Estimation of the surface tension of a solid: application to a liquid crystalline polymer. *Journal of Colloid and Interface Science*, 189(2), 361-369.

Daniel, G., Bardage, S., Fernando, D., Hafrén, J., Ander, P. (2009). Energy consumption in refining of Scots pine and Norway spruce TMP is governed by fibre morphology and ultrastructure. *International Mechanical Pulping Conference (IMPC)*, Sundsvall, Sweden.

Denes, A. R., Tshabalala, M. A., Rowell, R., Denes, F., Young, R. A. (1999). Hexamethyldisiloxane plasma coating of wood Surfaces for creating water repellent characteristics. *Walter de Gruyter, Holzforschung*, 53, 318-326.

De Vetter, L., Stevens, M., Van Acker, J. (2009a). Fungal decay resistance and durability of organosilicon-treated wood. *International Biodeterioration & Biodegradation*, 63, 130-134.

De Vetter, L., Van den Bulcke, J., De Windt, I., Stevens, M., Van Acker, J. (2009b). Preventive action of organosilicon treatments against disfigurement of wood under laboratory and outdoor conditions. *International Biodeterioration & Biodegradation*, 63, 1093-1101.

Derome, D., Roels, S., Carmeliet, J. (2005). Qualitative work to study water movement in wood. *7th Symposium on Building Physics in the Nordic Countries*, Reykjavik, Iceland.

Detter-Hoskin, L. D., Busch, K. L. (1995). SIMS: Secondary ion mass spectroscopy. In Conners, T. E., Banerjee, S. S., *Surface Analysis of Paper*. Inc. Boca Raton, Florida: CRC Press.

Dill-Langer, G., Lütze, S., Aicher, S. (2004). Microfracture in wood monitored by confocal laser scanning microscopy. *Wood Science and Technology*, 36(6), 487-499.

Donath, S., Militz, H., Mai, C. (2004). Wood modification with alkoxysilanes. *Wood Science and Technology*, 38(7), 555-566.

Donath, S., Militz, H., Mai, C. (2006). Creating water-repellent effects on wood by treatment with silanes. *Holzforschung*, 60, 40-46.

Donath, S., Militz, H., Mai, C. (2007). Weathering of silane treated wood. *Holz Roh Werkst*, 65, 35-42.

Duchesne, I., Geoffrey, D. (1999). The ultrastructure of wood fibre surfaces as shown by a variety of microscopical methods-a review. *Nordic Pulp and Paper Research Journal*, 14(2), 129-139.

Enomae, T., Yamaguchi, N., (2006). Influence of coating properties on paper-to-paper friction of coated paper, *Journal of Wood Science*, 52, 509-513.
Elowson, T., Bergström, M., Hämäläinen, M. (2003). Moisture dynamics in Norway spruce and Scots pine during outdoor exposure in relation to different surface treatments and handling conditions. *Holzforschung*, 57, 219–227.

Fahey, D. J., Pierce, D. S. (1971). Resistance of resin-impregnated paper overlays to accelerated weathering. *Forest Products Journal*, 21(11), 30-38.

Fardim, P., Gustafsson, J., Schoultz, S. V., Peltonen, J., Holmbom, B. (2005a). Extractives on fiber surfaces investigated by XPS, ToF-SIMS and AFM. *Colloids and Surfaces A: Physicochemical and Engineering Aspects*, 255, 91-103.

Fardim, P., Holmbom, B. (2005b). ToF-SIMS: a valuable chemical microscopy technique for paper and paper coatings. *Applied Surface Science*, 249, 393-407.

Fedel, M. (2010). *Environmentally friendly hybrid coatings for corrosion protection: silane based pre-treatments and nanostructured waterborne coatings*. Doctoral thesis, University of Trento, Italy.

Fernando, D., Daniel, G. (2008). Exploring pine fibre development mechanisms during TMP processing: Impact of cell wall ultrastructure (morphological and topochemical) on negative behavior. *Holzforschung*, 62, 597-607.

Fernando, D., Muhic, D., Engstrand, P., Geoffrey, D. (2011). Fundamental understanding of pulp property development under different thermomechanical pulp refining conditions as observed by a new Simon's staining method and SEM observation of the ultrastructure of fibre surfaces. *Holzforschung*, 65, 777-786.

Fengel, D., Wegener, G. (1989). *Wood-Chemistry, Ultrastructure, Reactions*. Walter de Gruyter, Berlin, Germany.

Finnish Thermowood Association (2003). *ThermoWood® handbook*, c/o Wood Focus Oy, Helsinki, Finland.

Forgacs, O. L., Atak, D. (1961). Distribution of chemical woodpulp and groundwood through the thickness of newsprint. In *The Formation and Structure of Paper*. Oxford: British Paper and Board Manufacturer Association.

Fowkes, F. M. (1964). Attractive forces at interfaces. *Journal of Industrial and Engineering Chemistry*, 56(12), 40-52.

Fromm, J., Rockel, B., Lautner, S., Windeisen, E., Wanner, G. (2003). Lignin distribution in wood cell walls determined by TEM and backscattered SEM techniques. *Journal of Structural Biology*, 143, 77-84.

Girifalco, L. A., Good, R. J. A. (1957). A theory for the estimation of surface and interfacial energies. 1. Derivation and application to interfacial tension. *Journal of Physical Chemistry*, 61, 904-909.

Good, R. J., Girifalco, L. A. (1960). A theory for estimation of surface and interfacial energies. 3. Estimation of surface energies of solids from contact angle data. *Journal of Physical Chemistry*, 64, 561-565.

Gustafsson, J. (2004). *Surface characterization of chemical and mechanical pulp fibres by AFM and XPS*. Doctoral thesis, Åbo Akademi University, Finland.

Hanley, S. J., Gray, D. G. (1994). Atomic force microscope images of black spruce wood sections and pulp fibers. *Holzforschung*, 48, 29-34.

Haugstad, G. (2012). *Atomic Force Microscopy: Understanding basic models and advanced applications.* Hoboken, New Jersey: John Wiley & Sons.

Hay, K. M., Dragila, M. I., Liburdy, J. (2008). Theoretical model for the wetting of a rough surface. *Journal of Colloid and Interface Science*, 325, 472-477.

Heikkurinen, A., Lucander, M., Sirviö, J., Varhimo, A. (1999). Effect of spruce wood and fiber properties on pulp quality under varying defibration conditions. *International mechanical pulping conference*, Houston.

Hietala, S., Maunu, S. L., Sundholm, F., Jämsä, S., Viitaniemi, P. (2002). Structure of thermaly modified wood studied by liquid state NMR measurements. *Holzforschung*, 56(5), 522-528.

Hill, C. (2006). *Wood modification-chemical, thermal and other processes*. West Sussex: John Wiley & Sons.

Iliev, S. D., Pesheva, N. C. (2003). Wetting properties of well-structured heterogeneous substrates. *Langmuir*, 19, 9923-9931.

ISO 25178. (2013). Retrieved October 28, 2013, from ISO 25178 – the free encyclopedia: http://en.wikipedia.org/wiki/ISO_25178

Iwamiya, Y., Yagi, O., Kinoshi, K. K. (2000). "Chouetsushi" a new transcendental type paper. *Annals of the High Performance Paper Society, Japan*, 39, 61-64.

Jang, H. F. (1998). Measurement of fibril angle in wood fibres with polarization confocal microscopy. *Journal of Pulp and Paper Science*, 24(7), 224-225.

Jayme, G., Harders-Steinhäuser, M. (1970a). Microscopy of wood and paper fibres. Microscopic staining procedures, In Freund, H., *Handbook of microscopy in technology*, Vol. V Microscopy of wood and paper, Part 2 Microscopy in technology of wood converting and wood degradation. Umschau-Verlag, Frankfurt/Main, 83-151.

Jayme, G., Harders-Steinhäuser, M. (1970b) Microscopy of wood and paper fibres. Application of different optical methods in fiber microscopy. In Freund, H., *Handbook of microscopy in technology*, Vol. V Microscopy of wood and paper, Part 2 Microscopy in technology of wood converting and wood degradation. Umschau-Verlag, Frankfurt/Main, 151-188.

Johnsen, P. O., Skinnarland, I., Helle, T., Houen, P. J. (1995). Distribution of lignin and other materials on particle surfaces in mechanical pulps. *International Mechanical Pulping Conference (IMPC)*, Ottawa, Canada.

Jämsä, S., Viitaniemi, P. (2001). Heat treatment of wood ─ Better durability without chemicals. *Proceedings of special seminar*, Antibes, France.

Järnström, J. (2010). *Topography and wetting of pigment coated substrates*. Doctoral thesis, Åbo Akademi University, Turku, Finland.

Kangas, H., Kleen, M. (2004). Surface chemical and morphological properties of mechanical pulp fines. *Nordic Pulp and Paper Research Journal*, 19(2), 191-199.

Kangas, H. (2007). *Surface chemical and morphological properties of mechanical pulps, fibers and fines*. Doctoral thesis, Helsinki University of Technology, Espoo, Finland.

Karnis, A. (1994). The mechanism of fibre development in mechanical pulping. *Journal of Pulp and Paper Science*, 20(10), J280-J288.

Kim, D. S., Bong, K. L., Yeo, J., Choi, M. J., Yang, W., Kwon, T. H. (2009). Fabrication of PDMS micro/nano hybrid surface for increasing hydrophobicity. *Microelectronic engineering*, 86, 1375-1378.

Kiuberis, J., Kazlauskas, R., Grabauskaite, L., Tautkus, S., Kareiva, A. (2003). Scanning electromicroscopy – a powerful tool for the characterization of materials. 2. Modified sol-gel chemistry approach to the conservation of paper. *Environmental and Chemical Physics*, 25(2), 81-85.

Kleen, M., Kangas, H., Laine, C. (2003). Chemical characterization of mechanical pulp fines and fiber surface layers. *Nordic Pulp and Paper Research Journal*, 18(4), 361-368.

Knop, A., Scheib, W. (1979). *Chemistry and Application of Phenolic Resins*. Berlin Heidelberg, New York: Springer Verlag.

Koljonen, K., Österberg, M., Johansson, L. -S., Stenius, P. (2003). Surface chemistry and morphology of different mechanical pulps determined by ESCA and AFM. *Colloids and Surfaces A: Physicochemical and Engineering Aspects*, 228, 143-158.

Koljonen, K. (2004). *Effect of surface properties of fibers on some paper properties of mechanical and chemical pulp*. Doctoral thesis, Helsinki University of Technology, Finland.

Kuusipalo, J. (2001). Plastic coating of plywood using extrusion technique. *Silva Fennica*, 35(1), 103-110.

Li, K., Lei, X., Lu, L., Camm, C. (2010). Surface characterization and surface modification of mechanical pulp fibres. *Pulp & Paper Canada*, 111(1), 28-33.

Li, K., Reeve, D. W. (2005). Analysis of lignin distribution across wood pulp fibre walls with confocal laser scanning microscopy. *Cellulose Chemistry and Technology*, 39(3), 211-223.

Lidbrandt, O., Mohlin, U. -B. (1980). Changes in fiber structure due to refining as revealed by SEM. *IPC International Symposium*: *On Fundamental Concepts of Refining*. Appleton, USA, 61-74.

Ly, B., Belgacem, M. N., Bras, J., Brochier Salon, M. C. (2010). Grafting of cellulose by fluorine-bearing silane coupling agents. *Materials Science and Engineering C*, 30, 343-347.

Mahlberg, R., Niemi, H. E. -M., Denes, F., Rowell, R. M. (1998). Effect of oxygen and hexamethyldisiloxane plasma on morphology, wettability and adhesion properties of polypropylene and lignocellulosics. *International Journal of Adhesion and Adhesives*, 18(4), 283-297.

Mahltig, B., Haufe, H., Böttcher, H. (2005). Functionalisation of textile by inorganic sol-gel coatings. *Journal of Materials Chemistry*, 15, 4385-4398.

Mai, C., Militz, H. (2004a). Modification of wood with silicon compounds. Inorganic silicon compounds and sol-gel systems: a review. *Wood Science and Technology*, 37, 339–348.

Mai, C., Militz, H. (2004b). Modification of wood with silicon compounds, Treatment systems based on organic silicon compounds – a review. *Wood Science and Technology*, 37, 453-461.

Meyer, G., Amer, N. M. (1990). Simultaneous measurement of lateral and normal forces with an optical-beam-deflection atomic force microscope. *Applied Physics Letters*, 57(20), 2089-2091.

Mork, E. (1928). Granvirkets kvalitet særlig med sigte paa slip- og celluloseved. *Papir Journalen*, 16(4), 40.

Militz, H., Beckers, E. P. J., Homan, W. J. (1997). Modification of solid wood: research and practical potential. The International Research Group on Wood Preservation, Whistler, Canada, Document Nr. IRG/WP 97-40098.

Minsky, M. (1988). Memoir on inventing the confocal scanning microscope. *Scanning*, 10(4), 128-138.

Molin, U., Daniel, G. (2004). Effects of refining on the fibre structure of kraft pulps as revealed by FE-SEM and TEM: Influence of alkaline degradation. *Holzforschung*, 58(3), 226-232.

Mosbye, J., Laine, J. and Moe, S. (2003). The effect of dissolved substances on the adsorption of colloidal extractives to fines in mechanical pulp. *Nordic Pulp and Paper Research Journal*, 18(1), 63-68.

Moss, P. A., Retulainen, E., Paulapuro, H., Aaltonen, P. (1993). Taking a new look at pulp and paper: applications of confocal laser scanning microscopy (CLSM) to pulp and paper research. *Paperi ja Puu-Paper and Timber*, 75(1-2), 74-79.

Mustaranta, A., Koljonen, K., Pere, J., Tenkanen, M., Stenius, P. and Buchert, J. (2000). Characterization of mechanical pulp fibres with enzymatic, chemical and immunochemical methods. *6th European Workshop on Lignocellulosics and Pulp (EWLP)*, Bordeaux, France, 15-18.

Nanko, H., Ohsawa, J. (1989). Mechanisms of bond formation. In Baker, C. F., Punton, V. W., *Fundamentals of paper-making*, Vol. I (Transactions of the 9th Fundamental research symposium, Cambridge, Sept. 1989). Mechanical Engineering Publications Ltd., London, 783-830.

Nosonovsky, M. (2007). Multiscale roughness and stability of superhydrophobic biomimetic interfaces. *Langmuir*, 23, 3157-3161.

Nuopponen, M., Vuorinen, T., Viitaniemi, P., Jämsä, S. (2003). Effects of heat treatment on the behaviour of extractives in softwood studied by FTIR spectroscopic methods. *Wood Science and Technology*, 37, 109–115.

Ogiso, K., Saka, S. (1993). Wood-inorganic composites prepared by sol-gel process II. Effects of ultrasonic treatments on preparation of wood-inorganic composites. *Mokuzai Gakkaishi*, 39, 301–307.

Oura, K., Lifshits, V. G., Saranin, A. A., Zotov, A. V., Katayama, M. (2001). *Surface Science: An introduction*. Berlin: Springer Verlag.

Owens, D. K., Wendt, R. C. (1969). Estimation of surface free energy of polymers. *Journal of Applied Polymer Science*, 13, 1741-1747.

Ozaki, Y., Bousfield, D. W., Shaler, S. M. (2005). Three-dimensional characterization of ink vehicle penetration by laser scanning confocal microscopy. *Journal of Pulp and Paper Science*, 31(1), 48-52.

Pachuta, S. J., Staral, J. S. (1994). Nondestructive analysis of colorants on paper by time-of-flight secondary ion mass spectrometry. *Analytical Chemistry*, 66(2), 276-284.

Panshin, A. J., deZeeuw, C. (1980). *Textbook of wood technology*, 4th ed. New York: McGraw-Hill.

Paulapuro, H. (2000). *Paper and Board grades*, Papermaking Science and Technology 18, Fapet Oy., Finland, 108–111.

Peltonen, J., Järn, M., Areva, S., Linden, M., Rosenholm, J. (2004). Topographical parameters for specifying a three-dimensional surface. *Langmuir*, 20, 9428-9431.

Peng, X., Zhong, L., Ren, J., Sun, R. (2010). Laccase and alkali treatments of cellulose fibre: Surface lignin and its influences on fibre surface properties and interfacial behavior of sisal fibre/phenolic resin composites. *Composites: Part A*, 41, 1848-1856.

Pfriem, A., Zauer, M., Wagenführ, A. (2009). Alteration of the pore structure of spruce (*Picea abies* (L.) Karst.) and maple (*Acer pseudoplatanus* L.) due to thermal treatment as determined by helium pycnometry and mercury intrusion porosimetry. *Holzforschung*, 63(1), 94–98.

Podgorski, L., Bousta, C., Schambourg, F., Maguin, J., Chevet, B. (2001). Surface modification of wood by plasma polymerization. *Pigment Resin Technol*ogy, 31, 33-40.

Pöhler, T., Heikkurinen, A. (2003). Amount and character of splits in the fiber cell wall caused by disc refining. *International mechanical pulping conference*, Quebec, 417-423.

Reme, P. A., Helle, T., Johnsen, P. O. (1998) Fibre characteristics of some mechanical pulp grades. *Nordic Pulp and Paper Research Journal*, 13(4), 263.

Ritschkoff, A. -C., Mahlberg, R., Suomi-Lindberg, L., Viikari, L., Nurmi, A. (2003). Properties of wood treated with hydrophobisation agents. *Proceedings of the first European Conference on Wood Modification*, Ghent.

Rowell, R. M. (2013). *Handbook of wood chemistry and wood composites*. Taylor & Francis, Florida: CRC press.

Rowell, R. M., Banks, W. B. (1985). Water repellency and dimensional stability of wood. United States Department of Agriculture, Forest Service, General Technical Report FPL-50.

Rowell, R. M., Youngs, R. L. (1981). Dimensional stabilization of wood in use. United States Department of Agriculture, Forest Service, Research Note FPL-0243.

Sain, M. (2000). X-ray photoelectron spectroscopy study of ultrathin-film-forming chemical-precursor-engineered lignocellulosic fiber and fiber-mat surfaces. *Applied Surface Science*, 158, 92-103.

Saka, S., Sasaki, M., Tanahashi, M. (1992). Wood-inorganic composites prepared by sol-gel processing I. Wood-inorganic composites with porous structure. *Mokuzai Gakkaishi*, 38, 1043–1049.

Saka, S., Ueno, T. (1997). Several $SiO_2$ wood-inorganic composites and their fire-resisting properties. *Wood Science and Technology*, 31, 457-466.

Saka, S., Miyafuji, H., Tanno, F. (2001). Wood-inorganic composites prepared by sol-gel process. *Journal of Sol-Gel Science and Technology*, 20, 213-217.

Singh, A. P., Dawson, B. S. W. (2004). Confocal microscope ─ a valuable tool for examining wood-coating interface. *JCT Research*, 1(3), 235-237.

Sjöström, E. (1993). *Wood Chemistry: Fundamentals and Applications*. New York: Academic Press.

Snell, R., Groom, L. H., Rials, T. G. (2001). Characterizing the surface roughness of thermomechanical pulp fibers with atomic force microscopy. *Holzforschung*, 55, 511-520.

Spori, D. M., Drobek, T., Zürcher, S., Ochsner, M., Sprecher, C., Mühlebach, A., Spencer, N. D. (2008). Beyond the lotus effect: roughness influences on wetting over a wide surface energy range. *Langmuir*, 24, 5411-5417.

Stamm, A. J., Hansen, L. A. (1937). Minimizing wood shrinkage and swelling. Effect of heating in various gases. *Industrial and Engineering Chemistry*, 29(7), 831-833.

Stenius, P., Koljonen, K. (2008). Surface characterization of mechanical pulp fibers by contact angle measurement, polyelectrolyte adsorption, XPS and AFM. In Hu, T. Q., *Characterization of Lignocellulosic Materials*. Blackwell, Oxford, 36-59.

Stout, K. J., Sullivan, P. J., Dong, W. P., Mainsah, E., Luo, N., Mathia, T., Zahouani, H. (1994). *The development of methods for the characterization of roughness on three*

*dimensions*. Commission of the European Communities: Luxembourg. Publication no. 15178 EN.

Stuart, B. H. (2004). *Infrared spectroscopy-Fundamentals and Applications*. John Wiley & Sons, New York.

Syrjänen, T, Kangas, E. (2000). Heat treated timber in Finland. International Research Group on Wood Preservation, Doc. No. IRG/WP 00-40158.

Tervala, O. (1999). Vanerin pinnoittaminen kestomuovilla. Lisensiaatintutkimus (in Finnish). Tampere University of Technology, Tampere.

Textor, T., Mahltig, B. (2010). A sol-gel based surface treatment for preparation of water repellent antistatic textiles. *Applied Surface Science*, 256, 1668-1674.

Tingaut, P., Weigenand, O., Mai, C., Militz, H., Sèbe, G. (2006). Chemical reaction of alkoxysilane molecules in wood modified with silanol groups. *Holzforschung*, 60, 271-277.

Tokareva, E. (2011). *Spatial distribution of components in wood by ToF-SIMS*. Doctoral thesis, Åbo Akademi University, Turku.

Tomšič, B., Simončič, B., Orel, B., Černe, L., Tavčer, P. F., Zorko, M., Jerman, I., Vilčnik, A., Kovač, J. (2008). Sol-gel coating of cellulose fibres with antimicrobial and repellent properties. *Journal of Sol-Gel Science and Technology*, 47, 44-57.

Trepte, J., Böttcher, H. (2000). Improvement in the leaching behavior of dye-doped modified silica layers coated onto paper or textiles. *Journal of Sol-Gel Science and Technology*, 19, 691-694.

Tshabalala, M. A., Kingshott, P., VanLandingham, M. R., Plackett, D. (2003a). Surface chemistry and moisture sorption properties of wood coated with multifunctional alkoxysilanes by sol-gel process. *Journal of Applied Polymer Science*, 88, 2828-2841.

Tshabalala, M. A., Gangstad, J. E. (2003b). Accelerated weathering of wood surfaces coated with multifunctional alkoxysilanes by sol-gel deposition. *Journal of Coatings Technology*, 75(943), 37-43.

Tshabalala, M. A., Sung, L. P. (2007). Wood surface modification by in-situ sol-gel deposition of hybrid inorganic-organic thin films. *Journal of Coatings Technology and Research*, 4(4), 483-490.

Tshabalala, M.A., Yang, V., Libert, R. (2009). Surface modification of wood by alkoxysilane sol-gel deposition to create anti-mold and anti-fungal characteristics. *Silanes and Other Coupling Agents*, 5, 135-147.

Vanoss, C. J., Chaudhury, M. K., Good, R. J. (1988). Interfacial Lifshitz-van der Waals and polar interactions in macroscopic systems. *Chemical Reviews*, 88(6), 927-941.

Viitaniemi, P., Jämsä, S., Ek, P., Viitanen, H. (1994). *Method for increasing theresistance of cellulosic products against mould and decay*. Pat. EP0695408. Appl. 94915166.6, 13.5.1994. Publ. 10.1.2001. 12p.

Wang, S., Mahlberg, R., Mannila, J., Nikkola, J., Jämsä, S., Ritschkoff, A. -C., Peltonen, J. (2011). Surface properties and moisture behaviour of pine and heat-treated spruce modified with alkoxysilanes by sol-gel process. *Progress in Organic Coatings*, 71, 274-282.

Wapner, P. G., Hoffman, W. P. (2002). Partial wetting phenomena on nonplanar surfaces and in shaped microchannels. *Langmuir*, 18, 1225-1230.

Werthmann, B. (1993a). Microscopic testing of chemical pulps, mechanical pulps, and paper. Microscopic staining methods, In Franke, W., *Testing of Paper, board, chemical pulp and mechanical pulp*, Vol. 2, Microscopical and photometrical testing procedures. Springer Berlin Heidelberg, 66-99.

Werthmann, B. (1993b). Microscopic testing of chemical pulps, mechanical pulps, and paper. Different microscopic procedures, In Franke, W., *Testing of Paper, board, chemical pulp and mechanical pulp*, Vol. 2, Microscopical and photometrical testing procedures. Springer Berlin Heidelberg, 146-156.

Wenzel, R. N. (1949). Surface roughness and contact angle, *Journal of Physical and Colloid Chemistry*, 53, 1466-1467.

Wise, L. E., Jahn, E. C. (1952). *Wood Chemistry*. Reinhold publishing company, United States of America.

Wu, S., Brzozowski, K. J. (1971). Surface free energy and polarity of organic pigments. *Journal of Colloid and Interface Science*, 37(4), 686-690.

Yagi, O., Iwamiya, Y., Suzuki, K. (2005). Improvement in tensile strength and water repellency of paper after treatment with methyltrimethoxysilane oligomer using titanium butoxide as a catalyst. *Journal of Sol-Gel Science and Technology*, 36, 69-75.

Yan, D., Li, K. (2008). Measurement of wet fiber flexibility by confocal laser scanning microscopy. *Journal of Materials Science*, 43, 2869-2878.

Ylikoski, J. (1992). *Characterization of fibre surface properties and fibrillation by confocal laser scanning microscopy*. M.Sc. Thesis, Helsinki University of Technology, Espoo, Finland.

Yoldas, B. E. (1998). Design of sol-gel coating media for ink-jet printing. *Journal of Sol-Gel Science and Technology*, 13(1-3), 147-152.

Zenkiewicz, M. (2007). Methods for the calculation of surface free energy of solids. *Journal of Achievements in Materials and Manufacturing Engineering*, 24(1), 137-145.

Zhu, Q., Gao, Q., Guo, Y., Yang, C. Q., Shen, L. (2011). Modified silica sol coatings for highly hydrophobic cotton and polyester fbarics using a one-step procedure. *Industrial & Engineering Chemistry Research*, 50, 5881-5888.

Österberg, M., Schmidt, U., Jääskeläinen, A. S. (2006). Combining confocal Raman spectroscopy and atomic force microscopy to study wood extractives on cellulose surfaces. *Colloids and Surfaces A: Physicochemical and Engineering Aspects*, 291, 197-201.

## APPENDIX

I SEM-EDS electron images (left) and Si maps (right) for the cross-sections of sol-gel A (MTEOS) and B (OTEOS) coated pine sapwood and heat-treated spruce

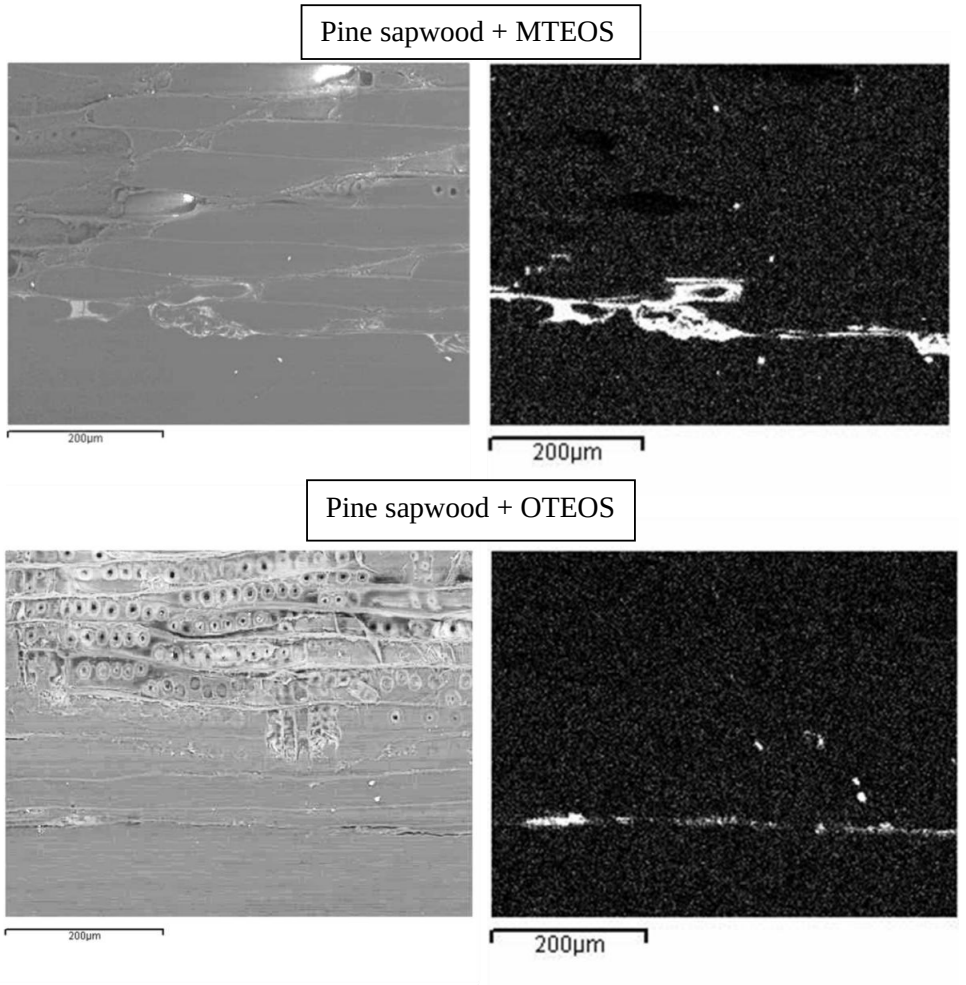

Heat-treated spruce + MTEOS

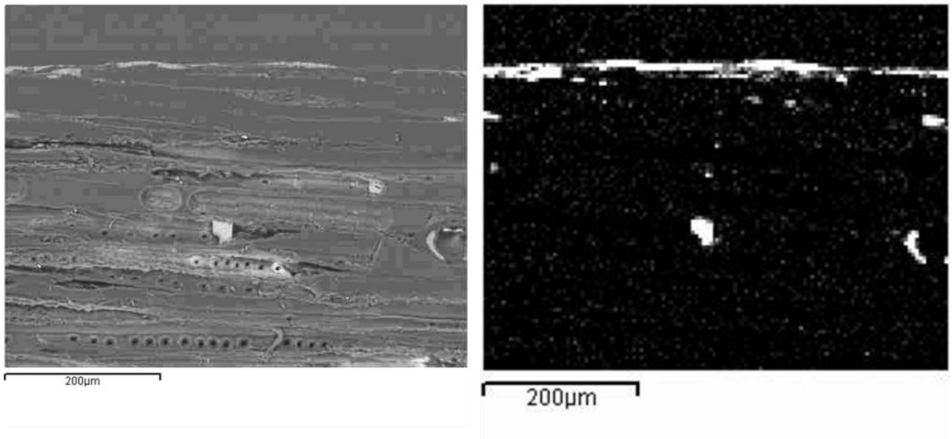


Heat-treated spruce + OTEOS

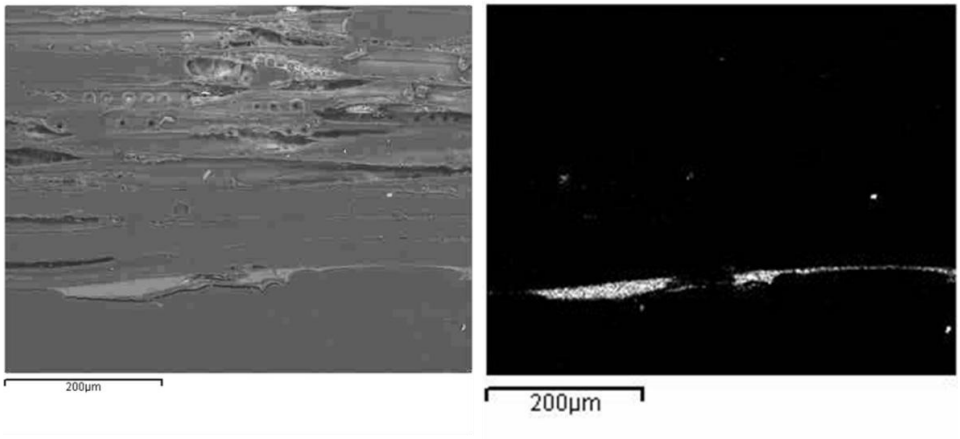

II SEM-EDS electron images (left) and Si maps (right) for the cross-sections of sol-gel A (MTEOS) and B (OTEOS) coated base paper and PF impregnated paper

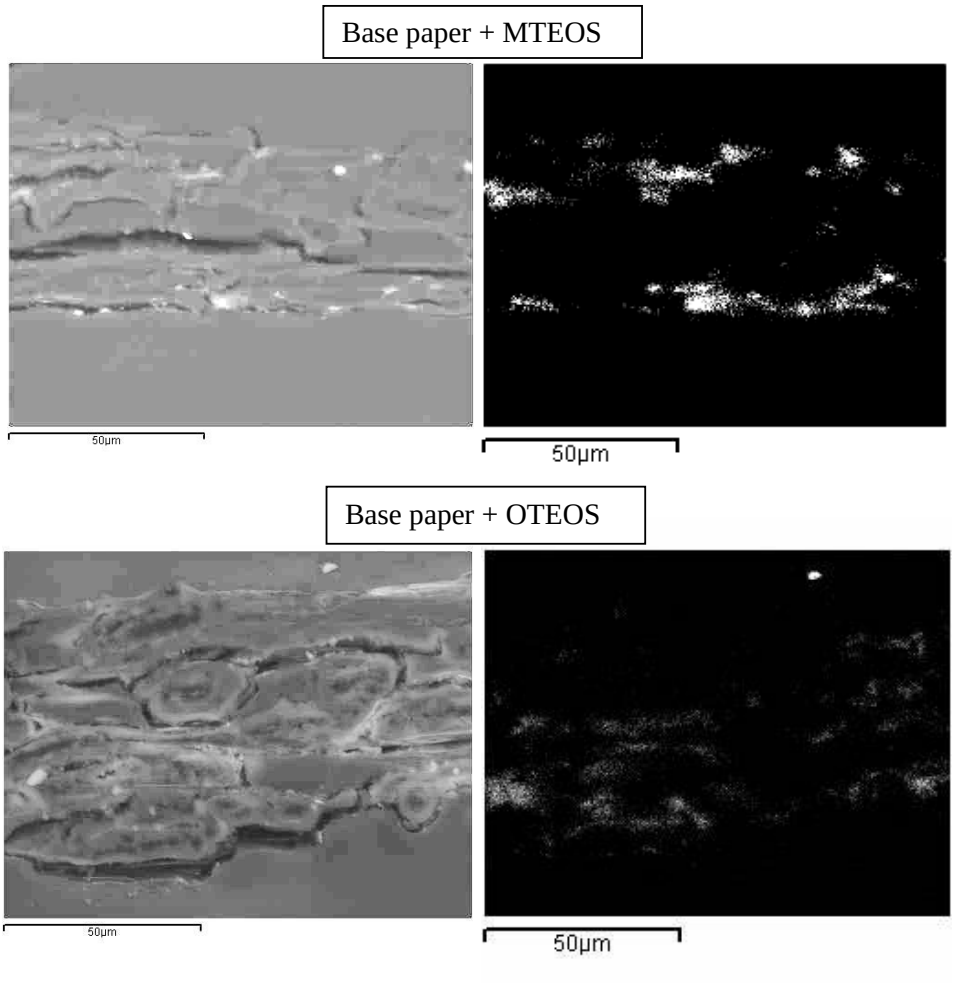

Impregnated paper + MTEOS

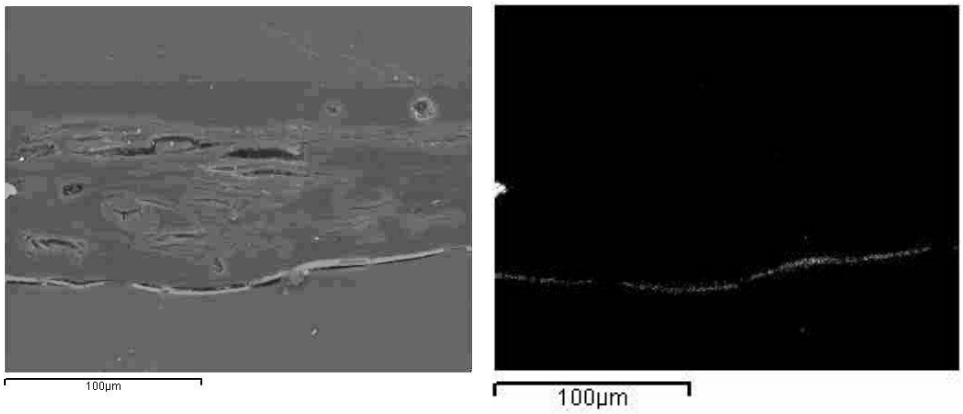


Impregnated paper + OTEOS

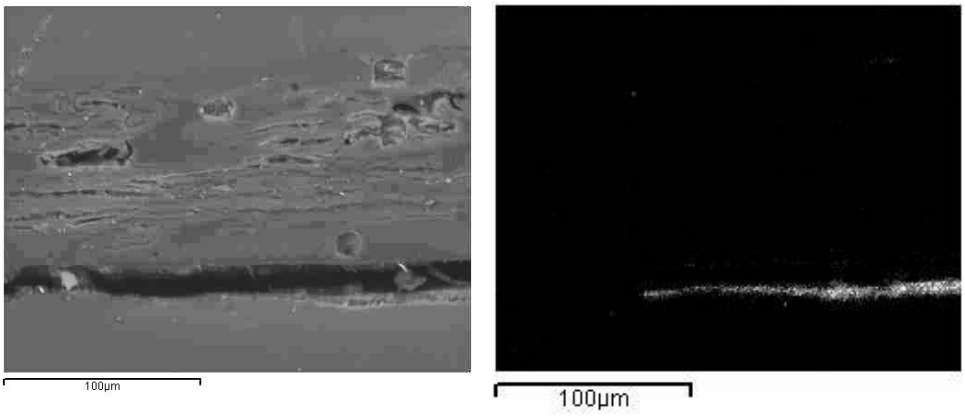

III SEM-EDS electron images (left) and Si maps (right) for the cross-sections of sol-gel B (OTEOS) and C (FTEOS) coated base paper and industrially impregnated paper

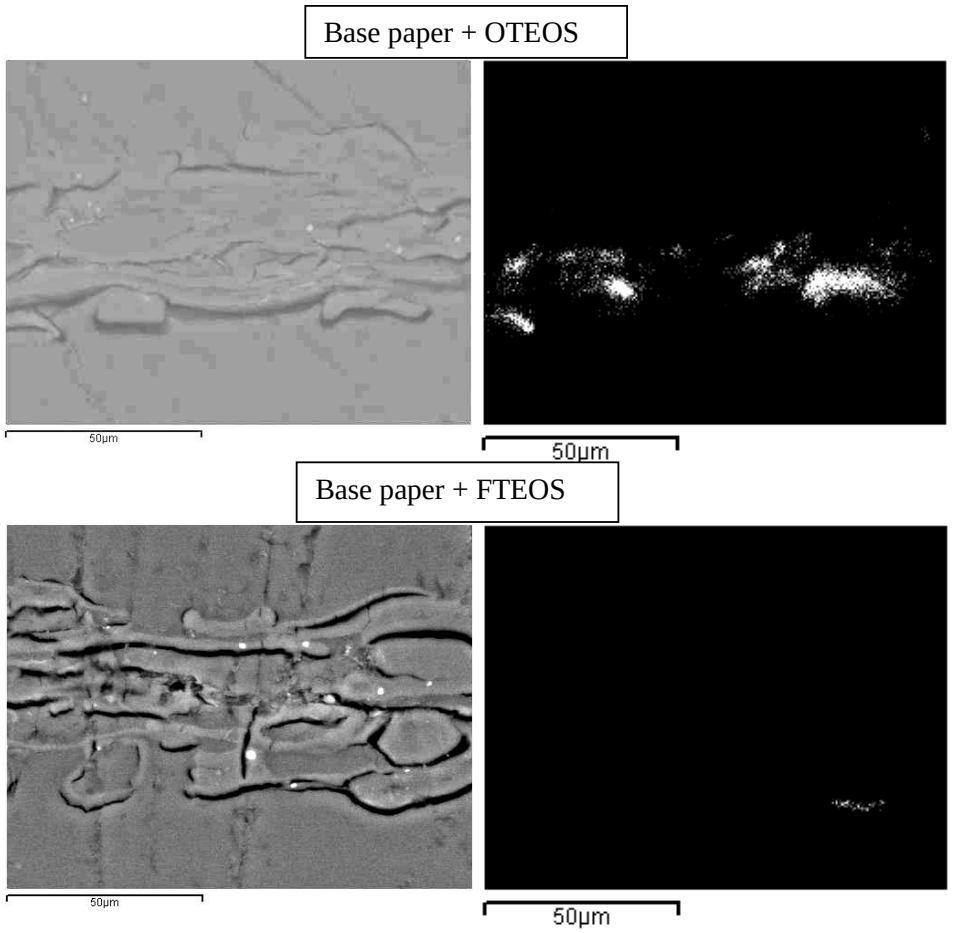

Impregnated paper + OTEOS

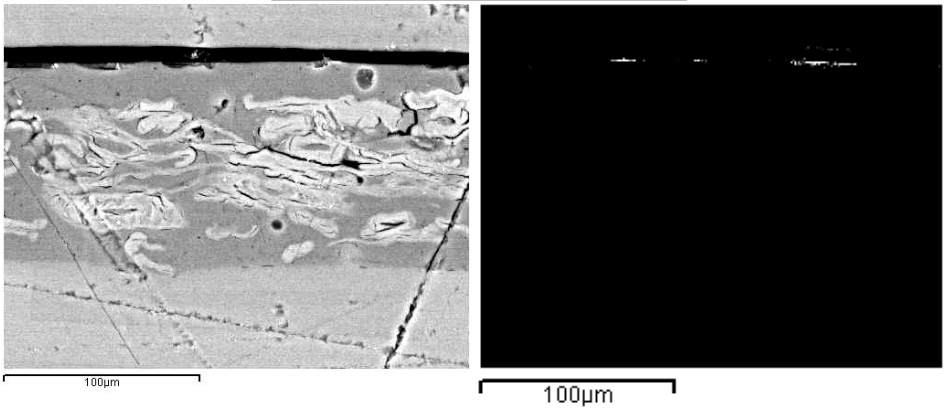


Impregnated paper + FTEOS

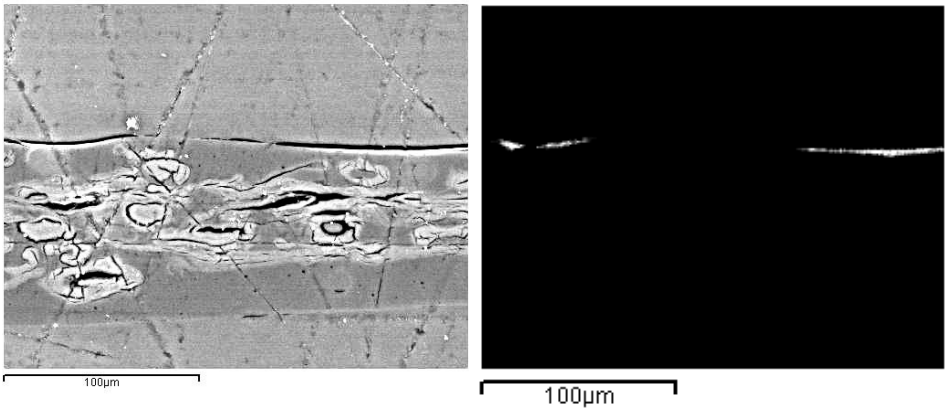






ISBN 978-952-12-3038-7